Exploring the effects of a double reconstruction on the growth rate of cosmic structure, using current observational data

Freddy Cueva Solano
Instituto de Física y Matemáticas, Universidad Michoacana de San Nicolás de Hidalgo
*Edificio C-3, Ciudad Universitaria, CP. 58040, Morelia, Michoacán, México.**

Based on General Relativity (GR) we consider two different cosmological scenarios in where reconstruct the energy exchange ($\bar{Q}$) between cold dark matter (DM) fluid and dark energy (DE) fluid, which is modelled with a DE varying equation of state (EoS) parameter ω. We here investigate the main cosmological effects on the growth rate of matter density perturbations ($f\sigma_8$), on the effective Hubble friction term (H_{eff}), on the effective Newton constant (G_{eff}) and on the growth index of the linear matter fluctuations (γ). Our study demonstrates that in the coupled models the evolution of these quantities are modified with respect to the predictions in the uncoupled models, and therefore could be used to distinguish among coupled DE scenarios. Finally, we also perform a combined statistical analysis using current observational data (geometric and dynamical probes) to put more stringent constraints on the parameters space of the cosmic scenarios studied.

PACS numbers: 98.80.-k, 95.35.+d, 95.36.+x, 98.80.Es

arXiv:1612.02484v1 [gr-qc] 7 Dec 2016

I. INTRODUCTION

The combined statistical analysis of the most recent measurements coming from JLA (Joint Light Curve Analysis) type Ia Supernovae (SNe Ia) data [1–3], the growth rate of structure formation obtained from redshift space distortion (RSD) data [4–23], the different Baryon Acoustic Oscillation (BAO) detected in the galaxy clustering observations (6dFGS, SDSS DR 7, SDSS DR 9, SDSS DR 11, BOSS DR 9 CMASS, 2dsPCF, 2dMPS, BOSS DR 11 CMASS), [19, 23–38], the observations of anisotropies in the power spectrum of the Cosmic Microwave Background (CMB: distance priors) data from the Planck 2015 data [23, 39–41], and the Hubble parameter (H) measurements obtained from galaxy surveys [42–51] indicate that the present universe is undergoing a phase of accelerated expansion. From the theoretical point of view, this phenomenon can be explained introducing in the universe an unknown physical fluid with negative pressure so-called DE [52–55]. Many alternative models have been suggested to explain it; in particular, the Lambda Cold Dark Matter (ΛCDM) model has a cosmological constant as DE with an EoS parameter $\omega = -1.0$ [56–59]. However, other more structured models replace Λ by a dynamical DE such as phantom model [60], quinton model [61], quintessence model [62], K-essence model [63], Chaplyging gas model [64], massive scalar field model [65], etc.

In the same way, within the universe we also assume the existence of another dark component so-called DM, which acts exactly like the ordinary matter (pressureless), and can interact with DE gravitationally.

On the other hand, the ΛCDM model presents two different problems such as the fine tuning and the cosmic coincidence. Then, one way to solve the last problem within GR is to assume a coupling between DE fluid and DM fluid. Currently, there are not neither physical arguments nor recent observations to exclude an energy exchange between these dark components because their natures are still unknown [66–81].

Due to the absence of a fundamental theory to construct $\bar{Q}$, different phenomenological parameterizations for $\bar{Q}$ have been proposed by mathematical simplicity [86]; for example, $\bar{Q} \propto \bar{H}\bar{\rho}_{DM}$ [69–72, 86], $\bar{Q} \propto \bar{H}\bar{\rho}_{DE}$ [70, 72, 82], $\bar{Q} \propto \bar{H}(\bar{\rho}_{DM} + \bar{\rho}_{DE})$ [70, 83–85], $\bar{Q} \propto \bar{\rho}_{DM}$ [71, 74] and $\bar{Q} \propto \bar{\rho}_{DE}$ [74]. Then such models may be physically viable, if they are confronted with the observational data, and therefore, can be employed in order to look new physical properties on cosmological scales [87–90].

On the other hand, the properties of DE fluid are mainly characterized by the EoS parameter ω. In this case, two possibilities are proposed to explain a varying ω. The first one is to parameterize ω in terms of some free-parameters [91–95]. Thus, among all the different ansatzes the Chevallier-Polarski-Linder (CPL) parameterization [92] $\omega = \omega_0 + \omega_1[z/(1+z)]$ (where z is the redshift, ω_0 and ω_1 are dimensionless parameters) is considered as the most popular ansatz. This ansatz shows a divergence problem when redshift z approaches to -1 [96]. The second one is to expand ω in terms of an appropriated local basis [97–100]. Consequently, we are interested in proposing a divergence-free reconstruction for ω and via a polynomial expansion, it will show new features. For example, we can expand ω, in function of the Chebyshev polynomials T_n, with $n \in N$. These polynomials are considered as a complete orthonormal basis on the finite interval $[-1, 1]$, and belong to the Hilbert space L^2 of real values [101]. Likewise, they have the property to be minimal approximately polynomials [44, 102], and possess a better advantage in terms of stability.

If we compare the theoretical predictions with the observational measurements, we will show the different effects of including the numerical reconstructions of $\bar{Q}$ and ω on the energy densities ($\bar{\Omega}_{DE}$ and $\bar{\Omega}_{DM}$), on the evolution of

* freddy@ifm.umich.mx, freddycuevasolano2009@gmail.com

the linear growth rate of DM density perturbation ($f\sigma_8$), on the effective Hubble friction term (H_{eff}) and on the effective Newton constant (G_{eff}), respectively. This will be the main aim of the present work.

On the other hand, RSD data represent a compilation of measurements of the quantity $f(z)\sigma_8(z)$ at different redshifts, which were obtained in a model independent way. These data are apparent anisotropies (effects) of the galaxy distribution (in redshift space), due to the differences of the estimates between the redshifts observed distances and true distances, and caused by the component along the line of sight (LOS) of the peculiar velocity of each of the galaxies (recessional velocity) [5, 103, 104]. Therefore, RSD data will provide tight constraints on the parameter space of the cosmic scenarios, and the necessary information to discriminate among all them [16, 17, 19, 21, 105–110].

Furthermore, another interesting observable considered here are the measurements of the Alcock-Paczynski (AP) effect [7]. This AP test describes a distortion along the observed tangential and radial dimensions of objects, which are assumed as isotropic [7, 111, 112]. This signal depends on the value of the F_{AP} parameter, and will be very useful to constrain cosmological models. In this work, the linear growth rate $f\sigma_8$ is constrained by measuring the RSD signal, while the dilation scale (D_v) [37] and F_{AP} parameter [7] evaluated at an effective redshift z_{eff} are constrained by measuring the BAO and AP signals, respectively.

Now then, two distinct coupled DE models such as XCPL and DR are studied here, and from which we have found a determined number of different effects such as a reduction or enhancement on the amplitudes of $\bar{\Omega}_{DE}$, $\bar{\Omega}_{DM}$, $f\sigma_8$, H_{eff} and G_{eff} at large and small redshifts with respect to those found in the uncoupled models. However, these modifications should be small in order to do not have a significant impact on the matter density perturbations. Furthermore, important features of the universe can be obtained from these changes, and therefore these variations depend of the chosen parameterizations for $\bar{Q}$ and ω, respectively. In this article, all our models are constrained using an analysis combined of JLA (SNe Ia) [1–3], the growth rate of structure formation obtained from RSD data [4–23], BAO data [19, 23–38], CMB data [23, 39–41] and the H data set [42–51].

Finally, we organize this paper as follows: The background equation of motions for the energy densities are presented in section II. In section III we describe the reconstruction schemes for $\bar{Q}$ and ω, respectively. In section IV we show the theoretical DE models. In section V we studied the conditions for the crossing of $\mathrm{I_Q} = 0$ line, and define the redshift crossing points. The perturbed equation of motions and the equations of structure formations are described in section VI. The current observational data and the priors considered are presented in section VII. We discuss our results in section VIII. In section IX, we conclude our main results.

II. BACKGROUND EQUATIONS OF MOTION

In a flat Friedmann-Robertson-Walker (FRW) universe its background dynamics is described by the following set of equations for their energy densities (detailed calculations are found in [86], so we do not discuss them here.)

$$\dot{\bar{\rho}}_b + 3\bar{H}\bar{\rho}_b = 0\,, \tag{1}$$

$$\dot{\bar{\rho}}_r + 4\bar{H}\bar{\rho}_r = 0\,, \tag{2}$$

$$\dot{\bar{\rho}}_{DM} + 3\bar{H}\bar{\rho}_{DM} = +\bar{Q}\,, \tag{3}$$

$$\dot{\bar{\rho}}_{DE} + 3\,(1+\omega)\,\bar{H}\bar{\rho}_{DE} = -\bar{Q}\,, \tag{4}$$

where $\bar{\rho}_b$, $\bar{\rho}_r$, $\bar{\rho}_{DM}$ and $\bar{\rho}_{DE}$ are the energy densities of the baryon, radiation, DM and DE, respectively. Now, defined the Hubble expansion rate as $\bar{H} \equiv \dot{a}/a$, and "$\cdot$" indicates differentiation with respect to the cosmic time t.

In what follows, we shall assume that there is not energy transfer from DE (DM) to baryon or radiation, and among them only exist a gravitational coupling [113]. For convenience, we defined the critical density $\rho_c \equiv 3\bar{H}^2/8\pi G$ and the critical density today $\rho_{c,0} \equiv 3H_0^2/8\pi G$ (in where H_0 is the current value of the Hubble parameter). Considering that $A = b, r, DM, DE$, and then the normalized densities become

$$\bar{\Omega}_A \equiv \frac{\bar{\rho}_A}{\rho_c} = \frac{\bar{\rho}_A/\rho_{c,0}}{\rho_c/\rho_{c,0}} = \frac{\Omega^\star_A}{E^2}\,, \qquad \Omega_{A,0} \equiv \frac{\rho_{A,0}}{\rho_{c,0}}\,. \tag{5}$$

The first Friedmann equation is given by

$$\begin{aligned} E^2 \equiv \frac{\bar{H}^2}{H_0^2} &= \frac{8\pi G}{3H_0^2}\left(\bar{\rho}_b + \bar{\rho}_r + \bar{\rho}_{DM} + \bar{\rho}_{DE}\right)\,, \\ &= \left[\Omega^\star_b + \Omega^\star_r + \Omega^\star_{DM} + \Omega^\star_{DE}\right]\,, \end{aligned} \tag{6}$$

and with the following relation for all time

$$\bar{\Omega}_b + \bar{\Omega}_r + \bar{\Omega}_{DM} + \bar{\Omega}_{DE} = 1\ . \tag{7}$$

The scale factor a is related to the redshift through $a = 1/(1+z)$, from which find $dt/dz = -1/(1+z)\bar{H}(z)$. Substituting this last relation into Eqs. (1)-(4), and solving Eqs. (1) and (2), we find

$$\Omega^\star_b(z) = \Omega_{b,0}(1+z)^3\,, \tag{8}$$

$$\Omega^\star_r(z) = \Omega_{r,0}(1+z)^4\,, \tag{9}$$

$$\frac{\mathrm{d}\Omega^\star_{DM}}{\mathrm{d}z} - \frac{3\,\Omega^\star_{DM}}{1+z} = \frac{-\Omega^\star_{DM}\mathrm{I_Q}(z)}{1+z}\,, \tag{10}$$

$$\frac{\mathrm{d}\Omega^\star_{DE}}{\mathrm{d}z} - \frac{3(1+\omega)\,\Omega^\star_{DE}}{1+z} = \frac{+\Omega^\star_{DM}\mathrm{I_Q}(z)}{1+z}\,. \tag{11}$$

These equations are fundamental to determine the results within our models.

III. PARAMETERIZATIONS OF $\bar{Q}$ AND w

The Chebyshev polynomials form a complete set of orthonormal functions on the interval $[-1, 1]$, and have the

property to be the minimal approximating polynomials. It is to say, they have the smallest maximum deviation from the true function at any given order [44, 86].
Because of the unknown of the origin and nature of the dark fluids, it is not possible to derive $\bar{Q}$ from fundamental principles, but we have the freedom of choosing any possible form of $\bar{Q}$ that satisfies Eqs. (10) and (11) simultaneously. Hence, we propose a phenomenological form for a varying Q, which could be definitely a function of $\bar{\rho}_{DM}$ multiplied both by a quantity with units of inverse of time (for instance $\bar{H}$) and by the coupling term, $\bar{\mathrm{I}}_{\mathrm{Q}}$. Since $\bar{\mathrm{I}}_{\mathrm{Q}}$ can be modelled as a varying function of z and used to measure the strength of the interaction, it can be reconstructed conveniently in terms of Chebyshev polynomials. Accordingly, we can look new physical properties in spite of the fact that $\bar{Q}$ may be determined by the universal expansion rate $\bar{H}$. Therefore, this scenario will simplify the analytic results, if we reconstruct $\bar{\mathrm{I}}_{\mathrm{Q}}$ from observational data. An energy exchange in the dark sector can be chosen as

$$\bar{Q} \equiv \bar{H}\bar{\rho}_{DM}\bar{\mathrm{I}}_{\mathrm{Q}} \, . \tag{12}$$

Here, the strength of the coupling is characterized by

$$\bar{\mathrm{I}}_{\mathrm{Q}} \equiv \sum_{n=0}^{2} \lambda_n T_n \, , \tag{13}$$

where the coefficients of the polynomial expansion λ_n are free dimensionless parameters [86], and

$$T_0(z) = 1 \, , \quad T_1(z) = z \, , \quad T_2(z) = (2z^2 - 1) \, , \tag{14}$$

represent the first three Chebyshev polynomials.
Within the CPL model, the past evolution history may be successfully described by its EoS parameter, ω, but the future evolution may not be explained, because ω grows increasingly, and then, encounters a divergence when $z \to -1$. That is not a physical feature. Consequently, to avoid such divergence problem we propose here a complete phenomenological reconstruction of a smoothly varying EoS parameter, ω, which can also be expanded in terms of an expansion of the Chebyshev polynomials such that

$$\omega(z) \equiv \omega_2 + 2\sum_{m=0}^{2} \frac{\omega_m T_m}{2 + z^2} \, , \tag{15}$$

where ω_0, ω_1 and ω_2 are free dimensionless parameters. The polynomial $(1 - 2z^2)^{-1}$ and the parameter ω_2 were included conveniently to simplify the calculations. However, this suitable generalization should be compatible with recent observational data. Likewise, $\omega(z)$ behaves nearly linear at low redshift $\omega(z = 0) = \omega_0$ and $d\omega/dz|_{z=0} = \omega_1$, whereas in the high redshift regime $\omega(z) \simeq 5\omega_2$.
The Chebyshev polynomials of order $m = 2$ were defined by Eq. (14). Thereafter, using numerical simulations we will compute the best fitted values for λ_0, λ_1, λ_2, ω_0, ω_1 and ω_2, respectively.

IV. DARK ENERGY MODELS

A. ΛCDM model

In this scenario, the function E^2 is defined fixing both $\omega(z) = -1$, and $\bar{Q}(z) = 0$ into Eqs. (8)-(11)

$$E^2 = \left[\Omega_b^{\star}(z) + \Omega_r^{\star}(z) + \Omega_{DM,0}(1+z)^3 + \Omega_{DE,0}\right] \, . \tag{16}$$

B. CPL model

Within this model, E^2 is determined replacing both $\omega(z) = \omega_0 + \omega_1[z/(1+z)]$, where ω_0, ω_1 are real parameters, and $\bar{Q}(z) = 0$ into Eqs. (8)-(11)

$$E^2 = \Bigg[\Omega_{b,0}(1+z)^3 + \Omega_{r,0}(1+z)^4 + \Omega_{DM,0}(1+z)^3 + \Omega_{DE,0}(1+z)^{3(1+\omega_0+\omega_1)}\exp\left(\frac{-3\omega_1 z}{1+z}\right)\Bigg] \, . \tag{17}$$

C. XCPL model

Firstly a coupled model can be defined putting both $\omega = \omega_0 + \omega_1(z/1+z)$, where ω_0, ω_1 are real free parameters, and $\bar{Q}(z)$ given by Eqs. (12) and (13) into Eqs. (8)-(11). The explicit form for $\Omega_{DM}^{\star}$ and $\Omega_{DE}^{\star}$ are reached by solving Eqs. (10) and (11), respectively.

$$\Omega_{DM}^{\star}(z) = (1+z)^3\Omega_{DM,0}\exp\left[\frac{-z_{max}}{2}\sum_{n=0}^{2}\lambda_n I_n(z)\right], \tag{18}$$

$$\Omega_{DE}^{\star}(z) = (1+z)^{3(1+\omega_0+\omega_1)}\Bigg[\Omega_{DE,0}\exp\left(\frac{-3\omega_1 z}{1+z}\right) + \frac{z_{max}}{2}\Omega_{DM,0}\exp\left(\frac{3\omega_1}{1+z}\right)\sum_{n=0}^{2}\lambda_n S_n(z,\bar{\omega})\Bigg] \, . \tag{19}$$

The following average integrals are also defined

$$\int_0^z \frac{T_n(\tilde{x})}{(1+\tilde{x})}d\tilde{x} \approx \frac{z_{max}}{2} I_n(z) \, , \tag{20}$$

$$\int_0^z \frac{T_n(\tilde{x})A(\tilde{x})B(\tilde{x})}{(1+\tilde{x})^{(1+3\omega_0+3\omega_1)}}d\tilde{x} \approx \frac{z_{max}}{2} S_n(z,\bar{\omega}) \, , \tag{21}$$

where we also defined the following expressions for all $n \in [0,2]$ (see Appendix A and [86])

$$
\begin{aligned}
A(\tilde{x}) &= \exp\left(\frac{-z_{max}}{2}\sum_{n=0}^{2}\lambda_n I_n(\tilde{x})\right) \,, \\
\tilde{A}(\tilde{x}) &= \exp\left(\frac{-z_{max}}{2}\sum_{n=0}^{2}\lambda_n \tilde{I}_n(\tilde{x})\right) \,, \\
B(\tilde{x}) &= \exp\left(\frac{-3\omega_1}{1+\tilde{x}}\right), \quad \tilde{B}(\tilde{x}) = \exp\left(\frac{-3\omega_1}{a+b\tilde{x}}\right), \\
I_n(z) &\equiv \int_{-1}^{x} \frac{T_n(\tilde{x})}{(a+b\tilde{x})} d\tilde{x} \,, \\
S_n(z,\bar{\omega}) &\equiv \int_{-1}^{x} \frac{T_n(\tilde{x})\tilde{A}(\tilde{x})\tilde{B}(\tilde{x})}{(a+b\tilde{x})^{(1+3\omega_0+3\omega_1)}} d\tilde{x} \,,
\end{aligned}
\tag{22}
$$

with the quantities

$$
x \equiv 2(z/z_{max}) - 1 \,, \quad a \equiv 1 + \frac{z_{max}}{2} \,, \quad b \equiv \frac{z_{max}}{2} \,,
$$

where z_{max} is the maximum value for z, and in which the observations are possible such that $\tilde{x} \in [-1,1]$ and $|T_n(\tilde{x})| \leq 1$, respectively.
Therefore, the function E^2 can be constructed from Eqs. (6), (8), (9), (18) and (19).

D. DR model

Secondly another coupled model can be modeled setting

$$
\omega(z) \equiv \omega_2 + 2\sum_{m=0}^{2}\frac{\omega_m T_m}{2+z^2} \,, \tag{23}
$$

where ω_0, ω_1 and ω_2 are real parameters. Moreover, $Q(z)$ is given by Eqs. (12) and (13). The analytic form for $\Omega^{\star}_{DM}$ can be reached by solving Eq. (10). For this model Eq. (18) represents the solution of Eq. (10). Instead, the solution of Eq. (11) can be obtained by numerical integration, from using Eq. (22) and Appendix A,

$$
\Omega^{\star}_{DE}(z) = C(z) + D(z)\int_{-1}^{x}\sum_{n=0}^{2}\lambda_n T_n(\tilde{x})\frac{F(\tilde{x})}{G(\tilde{x})}d\tilde{x} \,, \tag{24}
$$

where the following relations are defined

$$
\begin{aligned}
&C(z) = C_0(z).C_1(z).C_2(z) \,, \quad D(z) = D_0(z).D_1(z).D_2(z) \,, \quad F(\tilde{x}) = F_0(\tilde{x}).F_1(\tilde{x}).F_2(\tilde{x}) \,, \\
&C_0(z) = \Omega_{DE,0}(1+z)^{3(1+\omega_2)+A_0} \,, \quad C_1(z) = \left[\frac{(2z-z_{max})^2 + 2(z_{max}+2)^2}{3z_{max}^2 + 8(1+z_{max})}\right]^{A_1} \,, \\
&C_2(z) = \exp\left[A_2\sqrt{2}\left(\arctan\left[\frac{\sqrt{2}[2z-z_{max}]}{2z_{max}+4}\right] + \arctan\left[\frac{\sqrt{2}z_{max}}{2z_{max}+4}\right]\right)\right] \,, \\
&D_0(z) = 0.5 z_{max}\Omega_{DM,0}(1+z)^{2\omega_0-2\omega_1+5\omega_2+3}(2+z^2)^{\omega_1-\omega_0+5\omega_2} \,, \\
&D_1(z) = \exp\left[\sqrt{2}\Big(\omega_0+2\omega_1-5\omega_2\Big)\arctan\Big(0.5\sqrt{2}z\Big)\right] \,, \quad D_2(z) = \exp\left[\arctan\left(\frac{\sqrt{2}z_{max}}{4+2z_{max}}\right)J_2\right] \,, \\
&F_0(\tilde{x}) = \frac{\exp\left[-\sqrt{2}\Big(\omega_0+2\omega_1-5\omega_2\Big)\arctan\Big[0.25\sqrt{2}z_{max}(1+\tilde{x})\Big]\right]}{\left[(\tilde{x}^2+2)\,(0.5z_{max})^2 + 2\,(1+z_{max})\right]^{\omega_1-\omega_0+5\omega_2}} \,, \\
&F_1(\tilde{x}) = \left[\frac{\tilde{x}^2+2+8[z_{max}^{-2}+z_{max}^{-1}]}{3+8[z_{max}^{-2}+z_{max}^{-1}]}\right]^{J_1} \,, \quad F_2(\tilde{x}) = \exp\left[\arctan\left(\frac{\sqrt{2}z_{max}\tilde{x}}{2z_{max}+4}\right)J_2\right] \,, \\
&G(\tilde{x}) = \Big[1+0.5z_{max}(1+\tilde{x})\Big]^{2(\omega_0-\omega_1+\omega_2)-J_0} \,.
\end{aligned}
\tag{25}
$$

Within this model, the function E^2 can be constructed from Eqs. (6), (8), (9), (18) and (24). The basic analytical expressions for $A_n(x)$ and $J_n(\tilde{x})$ (when $n = 0,1,2$) are shown in Appendix A.

V. CROSSING OF $\bar{\mathrm{I}}_{\mathrm{Q}} = 0$ LINE WITH A MINIMAL DERIVATIVE COUPLING.

Let us now proceed with the calculation of the redshift crossing points, and analyze the behavior of $\bar{\mathrm{I}}_{\mathrm{Q}}$ and its

derived. From Eqs. (12), (13) and (14), we note that exist real values of z that lead to $\bar{\mathrm{I}}_{\mathrm{Q}}(z_{crossing}) = 0$

$$\bar{\mathrm{I}}_{\mathrm{Q}}(z_{crossing}) = 2\lambda_2 z_{crossing}^2 + \lambda_1 z_{crossing} + (\lambda_0 - \lambda_2) = 0. \tag{26}$$

in where the $z_{crossing}$ denotes the redshift crossing points of $\bar{\mathrm{I}}_{\mathrm{Q}} = 0$ line.
Then, the solution to Eq. (26) is given by

$$z_{crossing} = -\frac{\lambda_1}{4\lambda_2} \pm \sqrt{\left(\frac{\lambda_1}{4\lambda_2}\right)^2 - \left(\frac{\lambda_0 - \lambda_2}{2\lambda_2}\right)}. \tag{27}$$

From here, we note that these results depend of the choice for $\bar{\mathrm{I}}_{\mathrm{Q}}$. However, we are interested in the case where $\bar{Q} = 0$; in particular, this happens when $\bar{\mathrm{I}}_{\mathrm{Q}} = 0$. Furthermore, the reverse situation is also possible. In this discussion, to guarantee the possibility of the crossing of $\bar{\mathrm{I}}_{\mathrm{Q}} = 0$ line we must explore the function $\mathrm{d}\bar{\mathrm{I}}_{\mathrm{Q}}/\mathrm{d}z$. Now, we consider the possibility to have $\bar{\mathrm{I}}_{\mathrm{Q}} = 0$ and $\mathrm{d}\bar{\mathrm{I}}_{\mathrm{Q}}/\mathrm{d}z|_{z_{crossing}}$ could be zero or different of zero. Then, from Eqs. (13) and (14), we obtain

$$\frac{\mathrm{d}\bar{\mathrm{I}}_{\mathrm{Q}}}{\mathrm{d}z} = \lambda_1 + 4\lambda_2 z\,. \tag{28}$$

Substituting Eq. (27) into Eq. (28), we get the following

$$\frac{\mathrm{d}\bar{\mathrm{I}}_{\mathrm{Q}}}{\mathrm{d}z}|_{z_{crossing}} = \pm\frac{1}{4\lambda_2}\sqrt{{\lambda_1}^2 - 8\lambda_2(\lambda_0 - \lambda_2)} \neq 0\,, \tag{29}$$

Now, if we consider the possibility to have $\bar{\mathrm{I}}_{\mathrm{Q}}(z_{crossing}) = 0$ and $\mathrm{d}\bar{\mathrm{I}}_{\mathrm{Q}}/\mathrm{d}z|_{z_{crossing}} = 0$, it means that the impossibility for having $\bar{\mathrm{I}}_{\mathrm{Q}}$ over $\bar{\mathrm{I}}_{\mathrm{Q}} = 0$ line. By contrast, the only possibility for a crossing corresponds to

$$\bar{\mathrm{I}}_{\mathrm{Q}}|_{z_{crossing}} = 0 \qquad \frac{\mathrm{d}\bar{\mathrm{I}}_{\mathrm{Q}}}{\mathrm{d}z}|_{z_{crossing}} \neq 0. \tag{30}$$

From Eq. (29), we impose the following restraint for the avoidance of imaginary values in λ_1

$$\lambda_1 \geq \sqrt{8\lambda_2(\lambda_0 - \lambda_2)} \;\cup\; \lambda_1 \leq -\sqrt{8\lambda_2(\lambda_0 - \lambda_2)}\,, \tag{31}$$

which can be rewritten as

$$\mid \lambda_1 \mid \geq \sqrt{8\lambda_2(\lambda_0 - \lambda_2)}\,. \tag{32}$$

Similarly, from Eq. (32) to guarantee real values with physical sense, we impose

$$8\lambda_2(\lambda_0 - \lambda_2) \geq 0 \;\rightarrow \tag{33}$$
$$(\lambda_2 \geq 0) \cap (\lambda_0 \geq \lambda_2) \cup \tag{34}$$
$$(\lambda_2 \leq 0) \cap (\lambda_0 \leq \lambda_2)\,. \tag{35}$$

The values of $z_{crossing}$ for the coupled DE models are given in Table VII. Let us make some commentaries about the signs of $\bar{Q}$, $\bar{\mathrm{I}}_{\mathrm{Q}}$ and $\mathrm{d}\bar{\mathrm{I}}_{\mathrm{Q}}/\mathrm{d}z$, respectively. In general, if the parameters λ_0, λ_1 and λ_2 hold positive or negative values, then $\bar{\mathrm{I}}_{\mathrm{Q}}$ and $\mathrm{d}\bar{\mathrm{I}}_{\mathrm{Q}}/\mathrm{d}z$ will be ambiguously positive, negative or zero, in any epoch of the universe. From Eqs. (28), (32), (34) and (35), if λ_0 and λ_2 are both positive or are both negative, then $\mathrm{d}\bar{\mathrm{I}}_{\mathrm{Q}}/\mathrm{d}z$ could be positive or negative. Moreover, $\mathrm{d}\bar{\mathrm{I}}_{\mathrm{Q}}/\mathrm{d}z$ may be zero when λ_0, λ_1, and λ_2 are all zero (i.e. uncoupled DE models) or when $\mid \lambda_1 \mid = \sqrt{8\lambda_2(\lambda_0 - \lambda_2)}$. Here we can describe the signs of $\bar{Q}$ and $\bar{\mathrm{I}}_{\mathrm{Q}}$, choosing positive values for λ_0 either with negative values of λ_1 and positive values of λ_2 or with positive values of λ_1 and negative (positive) values of λ_2, in determined redshift ranges.

VI. PERTURBED EQUATIONS OF MOTION.

A. Perturbed equations of motion for coupled DE models.

Let us consider a spatially flat universe with scalar perturbations about the background. In the absence of the anisotropic stress, the perturbed line element in the Newtonian gauge is given by [74]

$$ds^2 = -(1+2\phi)\,dt^2 + a^2(t)\,(1-2\phi)\,d\vec{r}^{\,2}\,, \tag{36}$$

where ϕ is the gravitational potential, $a(t)$ is the scale factor, $U^\mu = \delta^\mu_0$ is the background four velocity, $U^\mu_A = (1-\phi, \partial^k v_A)$ or $U^A_\mu = (-(1+\phi), \partial_k v_A)$ is the A perfect-fluid four velocit, and v_A is the A fluid peculiar velocity potential. In addition, to avoid a momentum flux relative to U^μ_A, we define the total four velocity U^μ as [74]

$$U^\mu = (1-\phi, \partial^k v)\,, \tag{37}$$

where the total velocity potential v is given by [74]

$$(p+\rho)v = \sum_A (\bar{\rho}_A + \bar{p}_A) v_A, \tag{38}$$

with $\rho = \sum_A \bar{\rho}_A$, $P = \sum_A \bar{P}_A$ and $A = DM, DE, b, r$. This is the choice of v that we will use from now on. Thus, the A fluid energy-momentum tensor is [74]

$$T_A{}^{\mu\nu} = (\bar{\rho}_A + \bar{P}_A) U^\mu_A U^\nu_A + g^{\mu\nu}\bar{P}_A\,, \tag{39}$$

where $\rho_A = \bar{\rho}_A + \delta\rho_A$ and $P_A = \bar{P}_A + \delta P_A$. The covariant form of energy-momentum transfer is satisfied for the whole system, while for each component we have [74]

$$\nabla_\nu T_A{}^{\mu\nu} = F^\mu_A\,, \qquad \sum_A F^\mu_A = 0\,, \tag{40}$$

where F^μ_A describe the interaction, $F^\mu_A = 0$ for $A = (b,\, r)$ in the late universe, and $F^\mu_{DM} = -F^\mu_{DE} \neq 0$. A general F^μ_A relative to the total four velocity can be split as [74]

$$F^\mu_A = Q_A U^\mu + N^\mu_A\,, \tag{41}$$
$$Q_A = \bar{Q}_A + \delta Q_A\,, \tag{42}$$
$$u_\mu N^\mu_A = 0\,, \tag{43}$$

where Q_A is the energy density transfer and N^μ_A is the momentum density transfer rate, relative to U^μ_A. Here,

we also choose $N^{\mu}_{A}=(0,\partial^{k}f_{A})$, where f_{A} is a momentum transfer potential. Then, from Eq. (41) we find that [74]

$$F^{A}_{0}=-\left[\bar{Q}_{A}(1+\phi)+\delta Q_{A}\right]\,, \tag{44}$$

$$F^{A}_{k}=a^{2}\partial_{k}\left(f_{A}+\bar{Q}_{A}v\right). \tag{45}$$

The perturbed energy transfer F^{A}_{0} includes a metric perturbation term $\bar{Q}_{A}\phi$ and a perturbation δQ_{A}. In addition, we stress that the perturbed momentum transfer F^{A}_{k} is made up of two parts: the momentum transfer potential $\bar{Q}_{A}v$ that arises from energy transport along the total velocity and the intrinsic momentum transfer potential f_{A}. Hence, the total energy-momentum conservation implies that

$$\sum_{A}Q_{A}=\sum_{A}\delta Q_{A}=\sum_{A}f_{A}=0\,. \tag{46}$$

B. Structure formation in coupled DE models.

The general evolution equations for the dimensionless density perturbation $\delta_{A}=\delta\rho_{A}/\bar{\rho}_{A}$ is given by [67, 74, 75]

$$\dot{\delta}_{A}+3\bar{H}c^{2}_{SA}\delta_{A}-(1+w_{A})\frac{k^{2}}{a}v_{A}-3\bar{H}\left[3\bar{H}(1+w_{A})(c^{2}_{SA}-w_{A})+\dot{w}_{A}\right]v_{A}-3(1+w_{A})\dot{\phi}=\frac{\delta Q_{A}}{\bar{\rho}_{A}}+\frac{\bar{Q}_{A}}{\bar{\rho}_{A}}\left[\phi-\delta_{A}-3a\bar{H}(c^{2}_{SA}-w_{A})v_{A}\right], \tag{47}$$

also the velocity perturbation equation takes the form

$$\dot{v}_{A}+\bar{H}(1-3c^{2}_{SA})v_{A}+\frac{c^{2}_{SA}}{a(1+w_{A})}\delta_{A}+\frac{\phi}{a}=\frac{1}{(1+w_{A})\bar{\rho}_{A}}\left[\bar{Q}_{A}\left(v-(1+c^{2}_{SA})v_{A}\right)+f_{A}\right]\,, \tag{48}$$

and the relativistic Poisson equation is

$$\frac{k^{2}\phi}{a^{2}}=-3\bar{H}\dot{\phi}-3\bar{H}^{2}\phi-4\pi G\left(\bar{\rho}_{A}\delta_{A}\right)\,. \tag{49}$$

where G is Newton's constant.

We now consider that DE does not cluster on sub-Hubble scales $H\ll k/a$, and therefore, we could ignore $\dot{\delta}_{DE}$ from Eq. (47). Moreover, to avoid the nonphysical sound speed, we choose $c^{2}_{DE}=1$ [72, 115, 116].

Similarly, we also assume that the dynamical effects of the gravitational potential ϕ, its time derivative $\dot{\phi}$ and the transfer of energy between baryons and radiation, may be neglected relative to DM perturbation, δ_{DM}. Here, we also consider the case where DM component behaves as dust with an EoS parameter $\omega_{DM}=0$ and with a DM sound speed $c^{2}_{DM}=0$.

In the linear approach Eqs. (47) and (48) describe the evolution of the DM perturbation ($\delta_{DM}\ll 1$), which can be rewritten as [67, 74, 113]

$$\dot{\delta}_{DM}-\frac{k^{2}}{a}v_{DM}=\frac{\delta Q_{DM}}{\bar{\rho}_{DM}}-\frac{\bar{Q}_{DM}\delta_{DM}}{\bar{\rho}_{DM}}\,, \tag{50}$$

$$\dot{v}_{DM}+\bar{H}v_{DM}+\frac{\phi}{a}=\frac{1}{\bar{\rho}_{DM}}\left[\bar{Q}_{DM}(v-v_{DM})+f_{DM}\right]\,. \tag{51}$$

In this linear regime the Poisson equation reduces to

$$\frac{k^{2}\phi}{a^{2}}=-4\pi G\left(\bar{\rho}_{DM}\delta_{DM}+\bar{\rho}_{b}\delta_{b}\right). \tag{52}$$

In order to satisfy the weak equivalence principle and ensure that the particles of the DM can follow geodesics, we need to impose the following condition

$$f_{DM}=-\bar{Q}_{DM}(v-v_{DM})\,. \tag{53}$$

Here, Eq. (48) for DM component yields

$$\dot{v}_{DM}+\bar{H}v_{DM}+\frac{\phi}{a}=0\,. \tag{54}$$

This expression means that the DM velocity perturbation is not affected by the interaction with DE. Then, we provide a phenomenological covariant choice of the energy exchange four-vector

$$F^{\mu}_{DM}=-F^{\mu}_{DE}=Q_{DM}U^{\mu}_{DM}=(\bar{Q}_{DM}+\delta Q_{DM})U^{\mu}_{DM}\,, \tag{55}$$

in where one takes

$$\bar{Q}_{DM}=-\bar{H}\bar{\rho}_{DM}\bar{\mathrm{I}}_{\mathrm{Q}}\,, \tag{56}$$

$$\delta Q_{DM}=-\bar{\rho}_{DM}\bar{\mathrm{I}}_{\mathrm{Q}}\delta H-\bar{H}\bar{\mathrm{I}}_{\mathrm{Q}}\bar{\rho}_{DM}\delta_{DM}-\bar{H}\bar{\rho}_{DM}\delta\mathrm{I}_{\mathrm{Q}}. \tag{57}$$

We impose the following conditions $\delta\mathrm{I}_{\mathrm{Q}}\ll\delta_{DM}$ and $\delta\mathrm{I}_{\mathrm{Q}}\ll\delta H$ to generate DM cosmic structure formation

(In a forthcoming article we will extend our study, by considering other relations between $\delta \mathrm{I_Q}$, δ_{DM} and δH. It is beyond the scope of the present paper), so Eq. (57) becomes

$$\delta Q_{DM} = -\bar{\rho}_{DM}\bar{\mathrm{I}}_{\mathrm{Q}}\delta H - \bar{H}\bar{\mathrm{I}}_{\mathrm{Q}}\bar{\rho}_{DM}\delta_{DM}\,. \tag{58}$$

Considering that DM is more concentrated than the baryon component in the universe, also that DE does not cluster on sub-Hubble scales, using Eq. (6) and the relation $4\pi G\bar{\rho}_{DM} = 1.5\bar{H}^2\bar{\Omega}_{DM}$, we have

$$\delta H \approx \frac{\bar{H}}{2}\bar{\Omega}_{DM}\delta_{DM}\,, \tag{59}$$

and then,

$$\frac{\delta Q_{DM}}{\bar{\rho}_{DM}} - \frac{\bar{Q}_{DM}\delta_{DM}}{\bar{\rho}_{DM}} = \frac{\bar{H}}{2}\bar{\Omega}_{DM}\bar{\mathrm{I}}_{\mathrm{Q}}\delta_{DM}\,. \tag{60}$$

From Eqs. (51), (52), (54) and deriveting Eq. (50) with respect to t, we find the evolution of matter density perturbations $\delta_{DM}(t)$

$$\ddot{\delta}_{DM} + (2\bar{H} - \frac{1}{2}\bar{\Omega}_{DM}\bar{H}\bar{\mathrm{I}}_{\mathrm{Q}})\dot{\delta}_{DM} - \frac{3}{2}\bar{H}^2\bar{\Omega}_{DM}\delta_{DM}G_{eff} = 0, \tag{61}$$

When $\bar{\mathrm{I}}_{\mathrm{Q}} = 0$, Eq. (61) could be turner into the standard evolution of DM density perturbations. From this equation the quantity G_{eff} is an effective gravitational strength (effective Newton constant), defined as

$$G_{eff} \equiv G\left[1 + \frac{\bar{\mathrm{I}}_{\mathrm{Q}}^2}{3} + \frac{\dot{\bar{\mathrm{I}}}_{\mathrm{Q}}}{3H} + \frac{\bar{\mathrm{I}}_{\mathrm{Q}}}{6}(1 + 3w\bar{\Omega}_{DE})\right]. \tag{62}$$

which can be understood as a self attractive force acting on the DM density perturbation and quantifies the modifications to gravity due to the effects of $\bar{\mathrm{I}}_{\mathrm{Q}}$ and ω functions.
Here, we also define the effective Hubble friction term as

$$H_{eff} \equiv \bar{H}\left(1 - 0.25\bar{\Omega}_{DM}\bar{\mathrm{I}}_{\mathrm{Q}}\right). \tag{63}$$

which acts as a frictional force that slows down (reduces) the growth of cosmic structure.
It is useful to rewrite Eq. (61) in redshift space as

$$\delta_{DM}^{''} + \frac{\left(1 + 3\omega\Omega_{DE} + \bar{\Omega}_{DM}\bar{\mathrm{I}}_{\mathrm{Q}}\right)}{2(1+z)}\delta_{DM}^{'} - \frac{3\bar{\Omega}_{DM}G_{eff}}{2(1+z)^2}\delta_{DM} = 0 \tag{64}$$

$$G_{eff} \equiv G\left[1 + \frac{\bar{\mathrm{I}}_{\mathrm{Q}}^2}{3} - \frac{(1+z)}{3}\frac{d\bar{\mathrm{I}}_{\mathrm{Q}}}{dz} + \frac{\bar{\mathrm{I}}_{\mathrm{Q}}}{6}(1 + 3w\bar{\Omega}_{DE})\right]. \tag{65}$$

This equation can be solved numerically, considering that

$$\delta(z=0) = 1\,, \tag{66}$$

$$\delta^{'}(z=0) = -\Omega_{DM}(z=0)^{\gamma(z=0)}\,, \tag{67}$$

where γ is a some unknown function of z so-called the growth index of the linear matter fluctuations. In the linear regime, it is convenient to define the quantity

$$f \equiv \frac{dln\delta}{d\ln a} = -(1+z)\frac{d\ln\delta}{dz}\,, \tag{68}$$

called the growth factor of DM density perturbations. Then, Eq. (64) can be rewritten in function of f as

$$f^2 + \frac{1}{2}\left(1 - 3\omega\bar{\Omega}_{DE} - \bar{\Omega}_{DM}\bar{\mathrm{I}}_{\mathrm{Q}}\right)f - (1+z)\frac{df}{dz} \equiv \frac{3}{2}\frac{G_{eff}}{G}\bar{\Omega}_{DM} \tag{69}$$

This previous equation can be solved numerically, taking into account the condition $f(0) = \Omega_{DM}(z=0)^{\gamma(z=0)}$.
In full generality, we define the growth index of DM perturbations γ through the following ansatz

$$f \equiv \bar{\Omega}_{DM}^{\gamma(z)}(z)\,. \tag{70}$$

From Eq. (70), we find that

$$\frac{df}{dz} = \bar{\Omega}_{DM}^{\gamma}\left[\frac{d\gamma}{dz}\ln\bar{\Omega}_{DM} + \frac{\gamma}{\bar{\Omega}_{DM}}\frac{d\bar{\Omega}_{DM}}{dz}\right]. \tag{71}$$

Now, using Eqs. (1)-(4), we obtain

$$\frac{d\bar{\Omega}_{DM}}{dz} = -\frac{\bar{\Omega}_{DM}}{(1+z)}\left[\bar{\mathrm{I}}_{\mathrm{Q}} + 3\bar{\Omega}_{DE}\omega + \Omega_r\right]. \tag{72}$$

Substituting Eq. (72) into Eq. (71), we get

$$\frac{df}{dz} = \frac{\bar{\Omega}_{DM}^{\gamma}}{(1+z)}\left[(1+z)\frac{d\gamma}{dz}\ln\bar{\Omega}_{DM} - \gamma\left(\bar{\mathrm{I}}_{\mathrm{Q}} + 3\omega\bar{\Omega}_{DE} + \bar{\Omega}_r\right)\right]. \tag{73}$$

Let us now to equal Eqs. (69) and (73) to obtain the general evolution equation for the growth index γ

$$\frac{d\gamma}{dz} = \frac{1}{(1+z)\ln\bar{\Omega}_{DM}}\Bigg[\bar{\Omega}_{DM}^{\gamma} + \frac{1}{2} + \gamma(\bar{\mathrm{I}}_{\mathrm{Q}} + \bar{\Omega}_r) - \frac{\bar{\Omega}_{DM}\bar{\mathrm{I}}_{\mathrm{Q}}}{2} + 3\omega(1 - \bar{\Omega}_{DM} - \bar{\Omega}_b - \bar{\Omega}_r)(\gamma - \frac{1}{2}) + \frac{\bar{\Omega}_{DM}^{1-\gamma}}{2}\left((1+z)\frac{d\bar{\mathrm{I}}_{\mathrm{Q}}}{dz} - \frac{\bar{\mathrm{I}}_{\mathrm{Q}}}{2} - \bar{\mathrm{I}}_{\mathrm{Q}}^2 - 3 - \frac{3}{2}\omega\bar{\mathrm{I}}_{\mathrm{Q}}\left(1 - \bar{\Omega}_{DM} - \bar{\Omega}_b - \bar{\Omega}_r\right)\right)\Bigg]. \quad (74)$$

This equation can be solved numerically by considering the condition that $\gamma(z=0) = \gamma_0$.
The parameterization given by Eq. (70) is important to simplify rapidly the numerical calculations of Eqs. (69) and (74). Therefore, the DM linear growth factor normalized to unity at the present epoch is given by

$$g(z) = \frac{\delta_{DM}(z)}{\delta_{DM}(0)} = exp\left(-\int_0^z \bar{\Omega}_{DM}^{\gamma}(z)\frac{dz}{(1+z)}\right), \quad (75)$$

where z is the redshift of the universe in which the DM component dominates the universe (in this work for convenience used $z = 10$).
Let us stress that by solving numerically Eqs. (64) and (69) we can calculate δ_{DM} and f, respectively.
On the other hand, the root-mean-square amplitude of matter density perturbations within a sphere of radius $8\,Mpch^{-1}$ (being h the dimensionless Hubble parameter) is denoted as $\sigma_8(z)$ and its evolution is represented by

$$\sigma_8(z) = g(z)\sigma_8(z=0)\,. \quad (76)$$

in where $\sigma_8(z=0)$ is the normalization of $\sigma_8(z)$ today. Thus, the functions f y σ_8 can be combined to obtain $f\sigma_8$ at different redshifts. From here, we obtain

$$f(z)\sigma_8(z) = f(z)g(z)\sigma_8(z=0). \quad (77)$$

The measurements of $f\sigma_8$ will be important to constrain different cosmological models.

VII. CURRENT OBSERVATIONAL DATA AND COSMOLOGICAL CONSTRAINTS.

In this section, we describe how we use the cosmological data currently available to test and constrain the parameter space of our models proposed.

A. Join Analysis Luminous data set (JLA).

The SNe Ia data sample used in this work is the Join Analysis Luminous data set (JLA) [3] composed by 740 SNe with hight-quality light curves. Here, JLA data includes several low-redshift samples ($z < 0.1$), three samples from the Sloan Digital Sky Survey SDSS-II at $0.05 < z < 0.4$ and data from Supernova Legacy Survey (SNLS) in $0.2 < z < 1.0$.
For the JLA data, the observed distance modulus of each SNe is modeled by

$$\mu_i^{JLA} = m_{B,i}^* + \alpha x_{1,i} - \beta C_i - M_B\,, \quad (78)$$

in where $1 \leq z \leq 740$ and the parameters m_B^*, x_1 and C describe the intrinsic variability in the luminosity of the SNe, which are derived from the fitting of the light curves. Here, m_B^* is the observed peak magnitude in the rest-frame B band, x_1 is the stretch measure of the light-curve shape and C is the color measure for each SNe.
On the other hand, the nuisance parameters α, β, M and dM characterize the global properties of the light-curves of the SNe and are estimated simultaneously with the cosmological parameters of interest. The parameter α describes the luminosity of the light-curve, B represents the color-luminosity relationships, M is the absolute magnitude of the SNe in the rest-frame B band and dM denotes the correction of the absolute magnitude M with host galaxy properties. From here, we defined M_B

$$M_B = \begin{cases} M, & if\ \ \mathrm{M_{stellar}} < 10^{10}\mathrm{M}_{\odot}\,, \\ M + dM, & if\ \ \text{otherwise}\,, \end{cases} \quad (79)$$

where $\mathrm{M_{stellar}}$ is the host galaxy stellar mass, and $\mathrm{M}_{\odot}$ is the solar mass.
The total covariance matrix for this test is denoted as $C_{\mathbf{Betoule}}$, and can be written of the following manner

$$C_{\mathbf{Betoule}} = \sigma_{stat,\,ii}^2 + \sigma_{stat}^2 + \sigma_{sys}^2\,. \quad (80)$$

where $\sigma_{stat,\,ii}^2$, σ_{stat}^2 and σ_{sys}^2 denote the diagonal part of the statistical covariance matrix, the statistical covariance matrix and the systematic covariance matrix, respectively. The details of building of the matrix $C_{\mathbf{Betoule}}$ can be found in [1–3].

$$\sigma^2_{stat\,ii} = \sigma^2_{m^*_{B,i}} + \alpha^2\sigma^2_{x1,i} + \beta^2\sigma^2_{c,i} + 2\alpha Cov(m_{B,i}, x_{1,i}) - 2\beta Cov(m_{B,i}, c_i) - 2\alpha\beta Cov(x_{1,i}, c_i) + \sigma^2_{int} + \\ + \sigma^2_{lensing} + \sigma^2_{host\,correction} + \sigma^2_{z,i}\left[\frac{5(1+z_i)}{z_i(1+0.5z_i)\ln(10)}\right], \quad (81)$$

where the quantities $\sigma^2_{m^*_{B,i}}$, $\alpha^2\sigma^2_{x1,i}$ and $\beta^2\sigma^2_{c,i}$ are the covariances of m^*_B, x_1 and C for the i-th SNe, respectively, while $\alpha Cov(m_{B,i}, x_{1,i})$, $\beta Cov(m_{B,i}, c_i)$, and $\alpha\beta Cov(x_{1,i}, c_i)$ are the covariances between m^*_B, x_1 and C for each i-th SNe. The terms σ^2_{int}, $\sigma^2_{lensing}$ and $\sigma^2_{host\,correction}$ account for the uncertainty in cosmological redshift due to the following quantities: the peculiar velocities, the variation of magnitudes caused by gravitational lensing and the intrinsic variation in SNe magnitude, [1, 3]. We follow [1] in using $c\sigma_z = 150 kms^{-1}$ and the prescription suggested by Jönsson for $\sigma_{lensing} = 0.055z$ [2]. The values of $\sigma_{host\,correction}$ are compatible with a constant value of 0.106 ± 0.006 [3]. Furthermore, $\sigma^2_{z,i} = 0.0005$ denotes the covariance due to a peculiar velocity residual [1].
On the other hand, the theoretical distance modulus is defined as

$$\mu^{\rm th}(z, \mathbf{X}) \equiv 5\log_{10}\left[\frac{D_L(z, \mathbf{X})}{\rm Mpc}\right] + 25\,, \quad (82)$$

where the superscript "th" denotes the theoretical prediction for a SNe at a redshift z. Likewise, $D_L(z, \mathbf{X})$ is the luminosity distance, which in a FRW cosmology becomes

$$D_L(z_{hel}, z_{CMB}, \mathbf{X}) = (1+z_{hel})c\int_0^{z_{CMB}} \frac{dz'}{H(z', \mathbf{X})}\,, \quad (83)$$

where z_{hel} is the heliocentric redshift, z_{CMB} is the CMB rest-frame redshift, "c" is the speed of the light and $\mathbf{X}$ represents the cosmological parameters of the model. Considering that $c = 2.9999 \times 10^5 km/s$, so we rewrite $\mu^{\rm th}(z, \mathbf{X})$ as

$$\mu^{\rm th}(z_{hel}, z_{CMB}, \mathbf{X}) = 5\log_{10}\left[(1+z_{hel}\int_0^{z_{CMB}} \frac{dz'}{E(z', \mathbf{X})})\right] \\ +52.385606 - 5\log_{10}(H_0)\,. \quad (84)$$

Thus, the χ^2 distribution function for the JLA data is

$$\chi^2_{\mathbf{JLA}}(\mathbf{X}) = (\Delta\mu_i)^t\left(C^{-1}_{\mathbf{Betoule}}\right)_{ij}(\Delta\mu_j)\,, \quad (85)$$

where $\Delta\mu_i = \mu^{th}_i(\mathbf{X}) - \mu^{JLA}_i$ is a column vector of 740 entries of residuals between the theoretical and distance modulus. $C^{-1}_{\mathbf{Betoule}}$ is the 740×740 covariance matrix for all the observed distance modulus reported in [3], which contains information over both systematic and statistical errors.

B. RSD data

RSD data represent a compilation of measurements of the quantity $f(z)\sigma_8(z)$ at different redshifts, which were obtained in a model independent way. These data are apparent anisotropies (effects) of the galaxy distribution in redshift space due to the differences of the estimates between the redshifts observed distances and true distances. They are caused by the component along the line of sight (LOS) of the peculiar velocity of each of the galaxies (recessional speed). Thus, on very small scales (a few Mpc); especially, in the cores of the clustering of galaxies, the peculiar velocities of galaxies are almost randomly oriented such that the structures of the clustering appear elonged along the LOS when they are viewed in the redshift space (the "Finger of God" effect) [4] leading to a damping of the clustering of galaxies. By contrast, on large scale (from a few tens of Mpc to $100\,Mpc$) the observations show that the gravitational growth the galaxies tend to fall towards high-density regions and flow away from low-density regions such that the galaxy clustering in redshift space is enhanced in the LOS direction in comparison to the transverse direction [5].
The RSD test is an important probe for distinguishing cosmological DE models from standard cosmological models such as ΛCDM model; namely, different cosmological models might undergo similar background evolution behavior, but their growth histories of cosmic structures could be distinct in the coupled DE models.
In this work, we utilize the most recent growth rate data derived from redshift space distortions on the PSCz, 2dF, VVDS, 6dF, 2MASS, BOSS and WiggleZ galaxy surveys, and were collected by Mehrabi et al. (see Table in [6]). This sample is used to constrain the free parameters of our theoretical models.
The standard χ^2 for this data set is defined as [6]

$$\chi^2_{RSD}(\mathbf{X}) \equiv \sum_{i=1}^{18}\frac{\left[f{\sigma_8}^{th}(\mathbf{X}, z_i) - f{\sigma_8}^{obs}(z_i)\right]^2}{\sigma^2(z_i)}\,, \quad (86)$$

where $\sigma(z_i)$ is the observed 1σ uncertainty, $f{\sigma_8}^{\rm th}(\mathbf{X}, z_i)$ and $f{\sigma_8}^{obs}(z_i)$ represent the theoretical and observational growth rate, respectively.

C. BAO data sets

1. BAO I *data*

In this work, we make use of six different BAO galaxies clustering observations from six-degree-field galaxy

z	$f\sigma 8^{obs}$	σ	Refs.	z	$f\sigma 8^{obs}$	σ	Refs.
0.020	0.360	±0.0405	[11]	0.400	0.419	±0.041	[20]
0.067	0.423	±0.055	[12]	0.410	0.450	±0.040	[19]
0.100	0.370	±0.130	[13]	0.500	0.427	±0.043	[20]
0.170	0.510	±0.060	[14]	0.570	0.427	±0.066	[21]
0.220	0.420	±0.070	[19]	0.600	0.430	±0.040	[19]
0.250	0.351	±0.058	[18]	0.600	0.433	±0.067	[20]
0.300	0.407	±0.055	[20]	0.770	0.490	±0.180	[15, 17]
0.350	0.440	±0.050	[15, 16]	0.780	0.380	±0.040	[19]
0.370	0.460	±0.038	[18]	0.800	0.470	±0.080	[22]

TABLE I. Summary of RSD data set [11–22].

z	d_z^{obs}	σ_z	Refs.	z	d_z^{obs}	σ	Refs.
0.106	0.3360	±0.0150	[24, 25]	0.350	0.1161	±0.0146	[30]
0.150	0.2232	±0.0084	[26]	0.440	0.0916	±0.0071	[19]
0.200	0.1905	±0.0061	[19, 27]	0.570	0.0739	±0.0043	[31]
0.275	0.1390	±0.0037	[27]	0.570	0.0726	±0.0014	[32]
0.278	0.1394	±0.0049	[28]	0.600	0.0726	±0.0034	[19]
0.314	0.1239	±0.0033	[19]	0.730	0.0592	±0.0032	[19]
0.320	0.1181	±0.0026	[32]	2.340	0.0320	±0.0021	[34]
0.350	0.1097	±0.0036	[19, 27]	2.360	0.0329	±0.0017	[35]
0.350	0.1126	±0.0022	[29]				

TABLE II. Summary of BAO data set [19, 24–32, 34, 35].

survey (6dFGRS) [24, 25], the Sloan Digital Sky Survey (SDSS) Data Releases (DR) (such as SDSS-DR7 [19, 26–30], SDSS-DR9 [31, 33] and SDSS-DR11 [32], respectively.), the Wiggle Z dark energy survey [19] and the $Ly\alpha$ forest measurements from Baryon Oscillation Spectroscopic Data Release 11 (BOSS 11) [32, 34, 35]. Eisenstein et al. [36] and Percival et al. [27] constructed an effective distance ratio $D_v(z)$, which encodes the visual distortion of a spherical object due to the non-Euclidianity of a FRW spacetime. It is defined as

$$D_v(z,\mathbf{X}) \equiv \frac{1}{H_0}\left[(1+z)^2 {D_A}^2(z)\frac{cz}{E(z)}\right]^{1/3} , \\ = \frac{c}{H_0}\left[\left(\int_0^z \frac{dz'}{E(z',\mathbf{X})}\right)^2 \frac{z}{E(z,\mathbf{X})}\right]^{1/3} \quad (87)$$

where $D_A(z)$ is the proper (not comoving) angular diameter distance, which has the following definition

$$D_A(z,\mathbf{X}) \equiv \frac{c}{(1+z)}\int_0^z \frac{dz'}{H(z',\mathbf{X})} . \quad (88)$$

The comoving sound horizon size is defined by

$$r_s(a) \equiv c\int_0^a \frac{c_s(a')da'}{a'^2 H(a')} , \quad (89)$$

being $c_s(a)$ the sound speed of the photon-baryon fluid

$$c_s^2(a) \equiv \frac{\delta P}{\delta \rho} = \frac{1}{3}\left[\frac{1}{1+(3\Omega_b/4\Omega_r)a}\right] . \quad (90)$$

Considering Eqs. (89) and (90) for a z, we have

$$r_s(z) = \frac{c}{\sqrt{3}}\int_0^{1/(1+z)} \frac{da}{a^2 H(a)\sqrt{1+(3\Omega_{b,0}/4\Omega_{\gamma,0})a}} , \quad (91)$$

where $\Omega_{b,0}$ and $\Omega_{\gamma,0}$ are the present-day baryon and photon density parameters, respectively. In this paper, we have fixed $\Omega_{\gamma,0} = 2.469\times10^{-5}h^{-2}$, $\Omega_{b,0} = 0.02230h^{-2}$, and $\Omega_{r,0} = \Omega_{\gamma,0}(1+0.2271N_{eff})$, where N_{eff} represents the effective number of neutrino species (here, $\Omega_{b,0}$, $\Omega_{r,0}$ and the standard value, $N_{eff} = 3.04\pm0.18$ were chosen from Table 4 in [23]).

The epoch in which the baryons were released from photons is denoted as, z_d, and can be determined by using the following fitting formula [36]:

$$z_d = \frac{1291(\Omega_{M,0}h^2)^{0.251}}{1+0.659(\Omega_{M,0}h^2)^{0.828}}\left(1+b_1(\Omega_{b,0}h^2)^{b_2}\right) , \quad (92)$$

where $\Omega_{M,0} = \Omega_{DM,0} + \Omega_{b,0}$, and

$$b_1 = 0.313(\Omega_{M,0}h^2)^{-0.419}\left[1+0.607(\Omega_{M,0}h^2)^{0.674}\right] , \\ b_2 = 0.238(\Omega_{M,0}h^2)^{0.223} .$$

The peak position of the BAO depends of the distance radios d_z at different redshifts, which were obtained from the surveys already listed in Table II.

$$d_z(\mathbf{X}) = \frac{r_s(z_d)}{D_V(z,\mathbf{X})} , \quad (93)$$

where $r_s(z_d,\mathbf{X})$ is the comoving sound horizon size at the baryon drag epoch. From the data showed in Table II, we can build the χ^2 for the BAO I data

$$\chi^2_{\mathbf{BAO\,I}}(\mathbf{X}) = \sum_{i=1}^{17}\left(\frac{d_z^{th}(\mathbf{X},z_i) - d_z^{obs}(\mathbf{X},z_i)}{\sigma(\mathbf{X},z_i)}\right)^2 . \quad (94)$$

2. BAO II *data*

From BOSS DR 9 CMASS sample, Chuang et al. in [31] analyzed the shape of the monopole and quadrupole from the two-dimensional two-points correlation function 2d2pCF of galaxies and measured simultaneously $H(z)$, $D_A(z)$, $\Omega_m h^2$ and $f(z)\sigma_8(z)$ at the effective redshift $z = 0.57$. These results were $H(0.57) = 87.6\,^{+6.7}_{-6.8}$, $D_A(0.57) = 1396\pm73$, $\Omega_m h^2(0.57) = 0.126\,^{+0.008}_{-0.010}$ and $f(0.57)\sigma_8(0.57) = 0.428\pm0.066$. The units for H and D_A are $Kms^{-1}Mpc^{-1}$ and Mpc, respectively. Here, $\Delta A_i = A_i^{th}(\mathbf{X}) - A_i^{obs}$ is a column vector defined as

$$\Delta A_i = \begin{pmatrix} H(0.57)-87.6 \\ D_A(0.57)-1396 \\ \Omega_m h^2(0.57)-0.126 \\ f(0.57)\sigma_8(0.57)-0.428 \end{pmatrix} , \quad (95)$$

Then, the χ^2 function for the BAO II data is given by

$$\chi^2_{\mathbf{BAO\,II}}(\mathbf{X}) = (\Delta A_i)^t \left(C^{-1}_{\mathbf{BAO\,IV}}\right)_{ij} (\Delta A_j)\,, \qquad (96)$$

where the covariance matrix of measurements is listed in Eq. (26) of [31]

$$C^{-1}_{\mathrm{BAO\,II}} = \begin{pmatrix} +0.03850 & -0.0011410 & -13.53 & -1.2710 \\ -0.001141 & +0.0008662 & +3.354 & -0.3059 \\ -13.530 & +3.3540 & +19370 & -770.0 \\ -1.2710 & -0.30590 & -770.0 & +411.3 \end{pmatrix}. \qquad (97)$$

where "t" denotes its transpose.

3. BAO III *data*

Using SDSS DR 7 sample Hemantha et al [38], proposed a new method to constrain $H(z)$ and $D_A(z)$ simultaneously from the two-dimensional matter power spectrum 2dMPS without assuming a dark energy model or a flat universe. The values obtained at the effective redshift $z = 0.35$ were $H(0.35) = 81.3 \pm 3.8 Kms^{-1}Mpc^{-1}$, $D_A(0.35) = 1037 \pm 44 Mpc$ and $\Omega_m h^2(0.35) = 0.1268 \pm 0.0085$. They defined a column vector $\Delta B_i = B^{th}_i(\mathbf{X}) - B^{obs}_i$ as

$$B^{th}_i(\mathbf{X}) - B^{obs}_i = \begin{pmatrix} H(0.35,\mathbf{X}) - 81.3 \\ D_A(0.35,\mathbf{X}) - 1037.0 \\ \Omega_M h^2(0.35,\mathbf{X}) - 0.1268 \end{pmatrix}. \qquad (98)$$

The covariance matrix for the set of cosmological parameters under consideration was

$$C^{-1}_{\mathbf{BAO\,III}} = \begin{pmatrix} +0.00007225 & -0.169606 & +0.01594328 \\ -0.1696090 & +1936.0 & +67.030480 \\ +0.01594328 & +67.03048 & +14.440 \end{pmatrix}. \qquad (99)$$

The χ^2 function for the BAO III data set is written as

$$\chi^2_{\mathrm{BAO\,III}}(\mathbf{X}) = (\Delta B_i)^t \left(C^{-1}_{\mathbf{BAOIII}}\right)_{ij} (\Delta B_j)\,, \qquad (100)$$

where "t" denotes its transpose.

4. BAO IV *data*

In all the catalogs of galaxies, the positions of them are given in terms of angular positions and redshifts. In order to measure clustering of galaxies, we need to convert angular positions and redshifts of galaxies into physical positions, just for that we must use a fiducial cosmological model. These physical distances will depend on the chosen fiducial model. If the fiducial cosmology is significantly different from the real (true) cosmology, then this difference will induce any measured anisotropy, and should be used to constrain the true cosmology of the universe. This is known as the AP test. This signal affirms that if an astrophysical structure is spherically symmetric or isotropic, then it should possess equal comoving sizes, r_s, in parallel and transverse dimensions to the LOS [7]. Thus, the comoving diameter of a spherical object r_s at redshift z is related to its angular size $(\Delta\theta)$ on the sky by $\Delta\theta = r_s/[(1+z)D_A]$, which is known as observed transverse dimension, whilst the parallel dimension, r_s can also be related to the redshift difference by $\Delta z = r_s H(z)/c$. Furthermore, any difference between the relative values of z, $H(z)$ and D_A of an astrophysical structure in the fiducial cosmology and in the true cosmology, will manifest as anisotropies along the LOS. The parallel and transverse dimensions can be conveniently combined in a single parameter $F_{AP}(z)$, defined as

$$F_{AP}(z) = \frac{\Delta z}{\Delta\theta} = (1+z) D_A(z)\,(H(z)/c)\,, \qquad (101)$$

where $F_{AP}(z)$ is known as the AP distortion parameter. Measuring this parameter we can obtain accurate estimates of the angular distance $D_A(z)$ and Hubble parameter $H(z)$; likewise, we could break the degeneracy between them. For this reason, F_{AP} can also be used to constrain the properties of the DE [8].
It is convenient to report the results of the BAO peak, the AP test and the RSD effect, as joint measurements of $d_z(z_{eff})$, $F_{AP}(z_{eff})$ and $f(z_{eff})\sigma_8(z_{eff})$, where z_{eff} is an effective redshift. This joint measurements can be used to constrain cosmological parameters, and also, to distinguish different DE models. Then, we define a vector V with all these measurements at $z_{eff} = 0.57$, which can be built as [9, 10, 32]

$$\Delta V_i = V^{th}_i(\mathbf{X}) - V^{obs}_i = \begin{pmatrix} d_z(z_{eff}) - 13.880 \\ F_{AP}(z_{eff}) - 0.683 \\ f(z_{eff})\sigma_8(z_{eff}) - 0.422 \end{pmatrix}, \qquad (102)$$

The χ^2 function for this data set is fixed as

$$\chi^2_{\mathbf{BAO\,IV}}(\mathbf{X}) = (\Delta V_i)^t \left(C^{-1}_{\mathbf{BAO\,IV}}\right)_{ij} (\Delta V_j)\,, \qquad (103)$$

where the covariance matrix of measurements is listed in Eq. (1.3) of [9]

$$C^{-1}_{\mathrm{BAO\,IV}} = \begin{pmatrix} +31.032 & +77.773 & -16.796 \\ +77.773 & +2687.7 & -1475.9 \\ -16.796 & -1475.9 & +1323.0 \end{pmatrix}. \qquad (104)$$

Considering the Eqs. (94), (96), (100) and (103), we construct the total $\chi^2_{\mathbf{BAO}}$ for all the BAO data sets

$$\chi^2{}_{\mathbf{BAO}} = \chi^2_{\mathbf{BAO\,I}} + \chi^2_{\mathbf{BAO\,II}} + \chi^2_{\mathbf{BAO\,III}} + \chi^2_{\mathbf{BAO\,IV}}\,, \qquad (105)$$

D. CMB data set

The JLA (SNe Ia) and BAO data sets contain information about the universe at low redshifts, we now include

Planck 2015 data [23] to probe the entire expansion history up to the last scattering surface. The shift parameter $\mathbf{R}$ is provided by [39]

$$\mathbf{R}(z_*,\mathbf{X}) \equiv \frac{H_0}{c}\sqrt{\Omega_{M,0}}(1+z_*)D_A(z_*,\mathbf{X}), \\ = \sqrt{\Omega_{M,0}}\int_0^{z_*}\frac{d\tilde{y}}{E(\tilde{y})}\,, \tag{106}$$

where the distance D_A and $E(\tilde{y})$ are given by Eqs. (88) and (6), respectively. Moreover, the redshift z_* (the decoupling epoch of photons) is obtained using the following fitting function [40]

$$z_* = 1048\Big[1+0.00124(\Omega_{b,0}h^2)^{-0.738}\Big]\Big[1+g_1(\Omega_{M,0}h^2)^{g_2}\Big]\,, \tag{107}$$

where $\Omega_{M,0}=\Omega_{DM,0}+\Omega_{b,0}$, and

$$g_1 = \frac{0.0783(\Omega_{b,0}h^2)^{-0.238}}{1+39.5(\Omega_{b,0}h^2)^{0.763}}\,, \quad g_2 = \frac{0.560}{1+21.1(\Omega_{b,0}h^2)^{1.81}}. \tag{108}$$

An angular scale l_A for the sound horizon at decoupling epoch is defined as

$$l_A(\mathbf{X}) \equiv (1+z_*)\frac{\pi D_A(z_*,\mathbf{X})}{r_s(z_*,\mathbf{X})}\,, \tag{109}$$

where $r_s(z_*,\mathbf{X})$ is the comoving sound horizon at z_*, and is given by Eq. (91). Then, following [23, 41], the χ^2 for the CMB data is

$$\chi^2_{\mathbf{CMB}}(\mathbf{X}) = (\Delta x_i)^t\left(C^{-1}_{\mathbf{CMB}}\right)_{ij}(\Delta x_j)\,, \tag{110}$$

where $\Delta x_i = x_i^{th}(\mathbf{X}) - x_i^{obs}$ is a column vector

$$x_i^{th}(\mathbf{X}) - x_i^{obs} = \begin{pmatrix} l_A(z_*)-301.7870 \\ R(z_*)-1.7492 \\ z_*-1089.990 \end{pmatrix}\,, \tag{111}$$

"t" denotes its transpose and $(C^{-1}_{\mathbf{CMB}})_{ij}$ is the inverse covariance matrix [41] given by

$$C^{-1}_{\mathbf{CMB}} \equiv \begin{pmatrix} +162.48 & -1529.4 & +2.0688 \\ -1529.4 & +207232 & -2866.8 \\ +2.0688 & -2866.8 & +53.572 \end{pmatrix}\,. \tag{112}$$

The errors for the CMB data are contained in $C^{-1}_{\mathbf{CMB}}$.

E. Observational Hubble data (H)

Recently G. S. Sharov [42] compiled a list of 38 independent measurements of the Hubble parameter at different redshitfs, and used these measurements to constrain different cosmological models (see Table III in [42]). These data points were derived from two different methods: The first one includes twenty-five points, which were obtained from differential age dt for passively evolving galaxies with redshifts dz, (see [43–45, 49, 50])

$$\mathbf{H}(z) = -\frac{1}{1+z}\frac{dz}{dt}\,. \tag{113}$$

The second one contains 13 data points [30–32, 34, 35, 46–48, 51], and were determined by using the two-point correlation of Sloan Digital Sky Survey. Here, the BAO peak position was considered as a standard ruler in the radial direction.

The χ^2_H function for this data set is

$$\chi^2_{\mathbf{H}}(\mathbf{X}) \equiv \sum_{i=1}^{38}\frac{\left[H^{\rm th}(\mathbf{X},z_i,)-H^{obs}(z_i)\right]^2}{\sigma^2(z_i)}\,, \tag{114}$$

where $\mathbf{X}$ represents the parameters of the model, $H^{\rm th}$ is the theoretical value for the Hubble parameter, H^{obs} is the observed value, $\sigma(z_i)$ is the standard deviation measurement uncertainty, and the summation is over the 38 observational Hubble data at z_i. This test has been already used to constrain some models in [42].

Therefore, the best fitted parameters are obtained by minimizing the following total function χ^2,

$$\chi^2 = \chi^2{}_{\mathbf{JLA}}+\chi^2{}_{\mathbf{RSD}}+\chi^2{}_{\mathbf{BAO}}+\chi^2{}_{\mathbf{CMB}}+\chi^2{}_{\mathbf{H}}\,. \tag{115}$$

By means of this relation, we can construct the total probability density function, **pdf** as

$$\mathbf{pdf}(\mathbf{X}) = \mathrm{A}e^{-\chi^2/2}\,. \tag{116}$$

where A is a integration constant.

F. Constant Priors

In this work, we have assumed that baryonic matter (b) and radiation (r) are not coupled to DE or DM, which are separately conserved [113]. In this regard, we believe that the intensity of the interaction, $\mathrm{I_Q}$, is not affected by the values of $\Omega_{b,0}$ and $\Omega_{r,0}$, respectively. Thus, in this paper, we fixed: $\Omega_{\gamma,0}=2.469\times10^{-5}h^{-2}$ and $\Omega_{b,0}=0.02230h^{-2}$, given by Planck 2015 data [23]. Using these assumptions, in each of our models, we will construct a **pdf** function for them. The priors on the parameters space are given in Table IV, and were used in all our observational tests. From they we will compute the best fitting parameters.

VIII. RESULTS

We constructed a code to calculate numerically the theoretical evolutions of δ and f, respectively, and therefore, the values of $f\sigma_8$, setting functional forms on $\bar{\mathrm{I}}_{\mathrm{Q}}$ and ω such that they can be easily implemented in each of our models. Then, via a Markov Chain Monte Carlo (MCMC) analysis, we can perform a global fitting

z	$H(z)$	1σ	Refs.	z	$H(z)$	1σ	Refs.
0.070	69.0	±19.6	[43]	0.570	96.8	±3.40	[32]
0.090	69.0	±12.0	[44]	0.593	104.0	±13.0	[45]
0.120	68.6	±26.2	[43]	0.600	87.9	±6.1	[48]
0.170	83.0	±8.0	[44]	0.680	92.0	±8.0	[45]
0.179	75.0	±4.0	[45]	0.730	97.3	±7.0	[48]
0.199	75.0	±5.0	[45]	0.781	105.0	±12.0	[45]
0.200	72.9	±29.6	[43]	0.875	125.0	±17.0	[45]
0.240	79.69	±2.99	[46]	0.880	90.0	±40.0	[49]
0.270	77.0	±14.0	[44]	0.900	117.0	±23.0	[44]
0.280	88.8	±36.6	[43]	1.037	154.0	±20.0	[46]
0.300	81.7	±6.22	[47]	1.300	168.0	±17.0	[44]
0.340	83.8	±3.66	[46]	1.363	160.0	±33.6	[50]
0.350	82.7	±9.1	[30]	1.430	177.0	±18.0	[44]
0.352	83.0	±14.0	[45]	1.530	140.0	±14.0	[44]
0.400	95.0	±17.0	[44]	1.750	202.0	±40.0	[44]
0.430	86.45	±3.97	[46]	1.965	186.5	±50.4	[50]
0.440	82.6	±7.8	[48]	2.300	224.0	±8.6	[51]
0.480	97.0	±62.0	[49]	2.340	222.0	±8.5	[34]
0.570	87.6	±7.80	[31]	2.360	226.0	±9.3	[35]

TABLE III. Shows the observational $H(z)$ data [30–32, 34, 35, 43–51]

Parameters	Constant Priors
λ_0	$[-1.5\times10^{+2}, +1.5\times10^{+2}]$
λ_1	$[-1.5\times10^{+2}, +1.5\times10^{+2}]$
λ_2	$[-1.5\times10^{+1}, +1.5\times10^{+1}]$
ω_0	$[-2.0, -0.3]$
ω_1	$[-1.0, +1.0]$
ω_2	$[-2.0, +0.1]$
$\Omega_{DM,0}$	$[0, 0.7]$
$H_0(kms^{-1}Mpc^{-1})$	$[20, 120]$
α	$[-0.2, +0.5]$
β	$[+2.1, +3.8]$
M	$[-20, -17]$
dM	$[-1.0, +1.0]$
γ_0	$[+0.2, +1.2]$
σ_{80}	$[0, +1.65]$

TABLE IV. Shows the priors on the parameter space.

TABLE V. Shows the best fitting cosmological parameters for each model and their constraints at 1σ and 2σ obtained from an analysis of Union JLA+RSD+BAO+CMB+H data sets.

Parameters	ΛCDM	CPL	XCPL
λ_0	N/A	N/A	$+7.0\times10^{-4}{}^{+2.2609\times10^{-4}+4.5085\times10^{-4}}_{-1.9541\times10^{-4}-4.1348\times10^{-4}}$
λ_1	N/A	N/A	$-8.0\times10^{-4}{}^{+11.4167\times10^{-4}+25.3575\times10^{-4}}_{-8.7161\times10^{-4}-15.9322\times10^{-4}}$
λ_2	N/A	N/A	$+1.27\times10^{-5}{}^{+0.5128\times10^{-5}+1.1332\times10^{-5}}_{-0.4640\times10^{-5}-0.8529\times10^{-5}}$
ω_0	-1.0	$-1.0323^{+0.0489+0.1165}_{-0.0605-0.1586}$	$-1.0271^{+0.0563+0.1208}_{-0.0610-0.1497}$
ω_1	N/A	$+0.0952^{+0.1757+0.3024}_{-0.3267-0.9446}$	$+0.0950^{+0.2218+0.4488}_{-0.2827-0.7960}$
ω_2	N/A	N/A	N/A
$\Omega_{DM,0}$	$+0.2810^{+0.0185+0.0476}_{-0.0138-0.0279}$	$+0.2814^{+0.0176+0.0528}_{-0.0089-0.0154}$	$+0.2840^{+0.0308+0.0659}_{-0.0290-0.0542}$
$H_0(kms^{-1}Mpc^{-1})$	$+67.170^{+1.274+2.694}_{-1.3079-2.5666}$	$+67.19^{+1.3508+4.0403}_{-1.2203-3.3504}$	$+67.20^{+2.2767+5.3535}_{-1.6607-3.0699}$
α	$+0.1360^{+0.0419+0.0855}_{-0.0410-0.0814}$	$+0.1370^{+0.0787+0.1621}_{-0.0758-0.1542}$	$+0.1350^{+0.1017+0.2148}_{-0.0992-0.1993}$
β	$+3.068^{+0.1033+0.2129}_{-0.1026-0.2035}$	$+3.065^{+0.0434+0.0903}_{-0.0465-0.0897}$	$+3.078^{+0.1462+0.2953}_{-0.1556-0.3010}$
M	$-19.0340^{+0.3849+0.7605}_{-0.3907-0.7690}$	$-19.030^{+0.4560+0.9122}_{-0.4591-0.9179}$	$-19.0310^{+0.5241+1.0447}_{-0.5270-1.6457}$
dM	$-0.120^{+0.0299+0.2983}_{-0.2718-0.5360}$	$-0.121^{+0.2907+0.5838}_{-0.2975-0.5906}$	$-0.117^{+0.3290+0.6597}_{-0.3348-0.6634}$
γ_0	$+0.5511^{+0.0506+0.1010}_{-0.0375-0.0753}$	$+0.5510^{+0.0529+0.1088}_{-0.0506-0.0985}$	$+0.5510^{+0.0110+0.0298}_{-0.0010-0.0119}$
σ_{80}	$+0.8180^{+0.1400+0.2794}_{-0.1340-0.2718}$	$+0.8190^{+0.1471+0.2987}_{-0.1504-0.3036}$	$+0.8180^{+0.1643+0.3257}_{-0.1624-0.3213}$
χ^2_{min}	737.8591	736.8446	734.0572

Parameters	DR(1)	DR(2)
λ_0	$+1.12\times10^{-4}{}^{+0.6541\times10^{-4}+2.0752\times10^{-4}}_{-0.5693\times10^{-4}-1.4456\times10^{-4}}$	$+1.12\times10^{-4}{}^{+0.6541\times10^{-4}+2.0752\times10^{-4}}_{-0.5693\times10^{-4}-1.4456\times10^{-4}}$
λ_1	$+2.763\times10^{-4}{}^{+0.3867\times10^{-4}+0.7578\times10^{-4}}_{-0.5252\times10^{-4}-1.8572\times10^{-4}}$	$+2.763\times10^{-4}{}^{+0.3867\times10^{-4}+0.7578\times10^{-4}}_{-0.5252\times10^{-4}-1.8572\times10^{-4}}$
λ_2	$+2.540\times10^{-5}{}^{+1.0417\times10^{-5}+1.7126\times10^{-5}}_{-3.3311\times10^{-5}-3.8466\times10^{-5}}$	$-2.586\times10^{-5}{}^{+0.4648\times10^{-5}+0.9794\times10^{-5}}_{-1.1896\times10^{-5}-2.8076\times10^{-5}}$
w_0	$-1.0364^{+0.0644+0.1140}_{-0.0853-0.1908}$	$-1.0364^{+0.0644+0.1140}_{-0.0853-0.1908}$
w_1	$+2.1064^{+0.2363+0.5842}_{-0.1213-0.1964}$	$+2.1064^{+0.2363+0.5842}_{-0.1213-0.1964}$
w_2	$-0.7698^{+0.1276+0.4797}_{-0.0364-0.0717}$	$-0.7698^{+0.1276+0.4797}_{-0.0364-0.0717}$
$\Omega_{DM,0}$	$+0.2844^{+0.0121+0.0385}_{-0.0061-0.0124}$	$+0.2844^{+0.0121+0.0385}_{-0.0061-0.0124}$
$H_0(kms^{-1}Mpc^{-1})$	$+67.1490^{+0.8216+1.8006}_{-0.9642-1.9324}$	$+67.1490^{+0.8216+1.8006}_{-0.9642-1.9324}$
α	$+0.1360^{+0.1108+0.2341}_{-0.1198-0.2482}$	$+0.1360^{+0.1108+0.2341}_{-0.1198-0.2482}$
β	$+3.0780^{+0.1968+0.3939}_{-0.1839-0.370}$	$+3.0780^{+0.1968+0.3939}_{-0.1839-0.3700}$
M	$-19.1650^{+0.5561+1.1116}_{-0.5522-1.0996}$	$-19.1650^{+0.5561+1.1116}_{-0.5522-1.0996}$
dM	$-0.120^{+0.3742+0.7492}_{-0.3740-0.7536}$	$-0.120^{+0.3742+0.7492}_{-0.3740-0.7536}$
γ_0	$+0.5511^{+0.0302+0.0615}_{-0.0291-0.0571}$	$+0.5511^{+0.0302+0.0615}_{-0.0291-0.0571}$
σ_{80}	$+0.8190^{+0.1706+0.3425}_{-0.1690-0.3417}$	$+0.8190^{+0.1706+0.3425}_{-0.1690-0.3417}$
χ^2_{min}	731.7439	734.3817

in each of them (listed in Table V), by using a combined statistical analysis of cosmic observations such as JLA

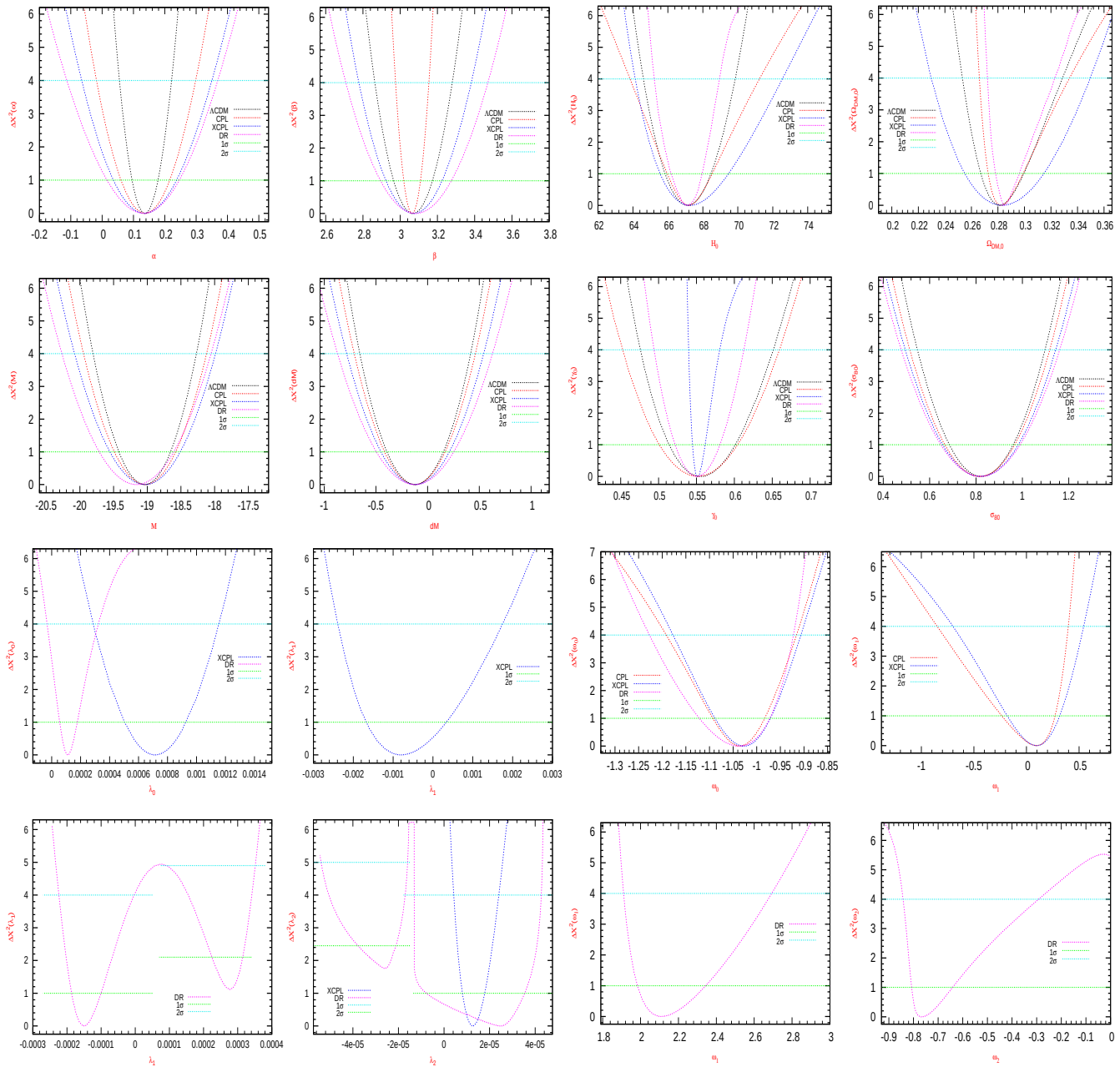

FIG. 1. (color online) Displays the one-dimension probability contours for all the parameters worked and their constraints at 1σ and 2σ, respectively. Moreover, we consider that $\Delta\chi^2 = \chi^2 - \chi^2_{min}$.

TABLE VI. Shows the best fitting cosmological parameters today, $f\sigma_{8,0}$, γ_0, $\mathrm{I}_0 \times 10^4$, ω_0, $\Omega_{DM,0}$, $G_{eff,0}$, $H_{eff,0}$ and their errors at 1σ obtained from a combination of data.

Models	$f\sigma_{8,0}$	γ_0	$\mathrm{I}_0 \times 10^4$	ω_0	$\Omega_{DM,0}$	$G_{eff,0}$	$H_{eff,0}$
ΛCDM	$+0.4037^{+0.0571}_{-0.0587}$	$+0.5506^{+0.0527}_{-0.0390}$	0.0	-1.0	$+0.2810^{+0.0185}_{-0.0138}$	$+1.0$	$+2.0$
CPL	$+0.4049^{+0.0580}_{-0.0585}$	$+0.5505^{+0.0551}_{-0.0527}$	0.0	$-1.0323^{+0.0489}_{-0.0605}$	$+0.2819^{+0.0171}_{-0.0094}$	$+1.0$	$+2.0$
XCPL	$+0.4063^{+0.1035}_{-0.0965}$	$+0.5506^{+0.0114}_{-0.0069}$	$+6.8730^{+2.2096}_{-1.9077}$	$-1.0271^{+0.0563}_{-0.0610}$	$+0.2840^{+0.0308}_{-0.0290}$	$+1.000146^{+3.07\times10^{-4}}_{-3.9\times10^{-4}}$	$+1.999902^{+3.5\times10^{-5}}_{-4.5\times10^{-5}}$
DR(1)	$+0.4070^{+0.0781}_{-0.0758}$	$+0.5507^{+0.0313}_{-0.0302}$	$+0.8660^{+0.5543}_{-0.2362}$	$-1.0364^{+0.0644}_{-0.0853}$	$+0.2844^{+0.0121}_{-0.0061}$	$+0.999892^{+2.0\times10^{-5}}_{-1.9\times10^{-5}}$	$+1.999988^{+3.0\times10^{-6}}_{-9.0\times10^{-6}}$
DR(2)	$+0.4070^{+0.0781}_{-0.0758}$	$+0.5507^{+0.0313}_{-0.0302}$	$+1.3786^{+0.6070}_{-0.4503}$	$-1.0364^{+0.0644}_{-0.0853}$	$+0.2844^{+0.0121}_{-0.0061}$	$+0.999883^{+2.3\times10^{-5}}_{-1.8\times10^{-5}}$	$+1.999980^{+7.0\times10^{-6}}_{-9.0\times10^{-6}}$

data, the RSD data, the BAO data, the CMB given by the Planck 2015 data and the H data; from which, we

TABLE VII. Shows the z_{cross} points and the values of $f\sigma_8$, γ, $\bar{\mathrm{I}}_{\mathrm{Q}}$, ω, Ω_{DM}, G_{eff}, H_{eff} evaluated at z_{cross}.

Models	z_{cross}	$f\sigma_8(z_{cross})$	$\gamma(z_{cross})$	$\omega(z_{cross})$	$\Omega_{DM}(z_{cross})$	$G_{eff}(z_{cross})$	$H_{eff}(z_{cross})$
XCPL	$+0.8886$	$+0.4348$	$+0.4734$	-0.9824	$+0.6571$	$+1.000475$	$+2.0$
DR1	-0.3342	$---$	$---$	-1.8518	$+0.1281$	$+0.999946$	$+2.0$
DR2	-0.4593	$---$	$---$	-2.1799	$+0.080$	$+0.999940$	$+2.0$
DR2	$+5.8073$	$+0.1949$	-14.7150	-3.0065	$+0.8357$	$+1.000736$	$+2.0$

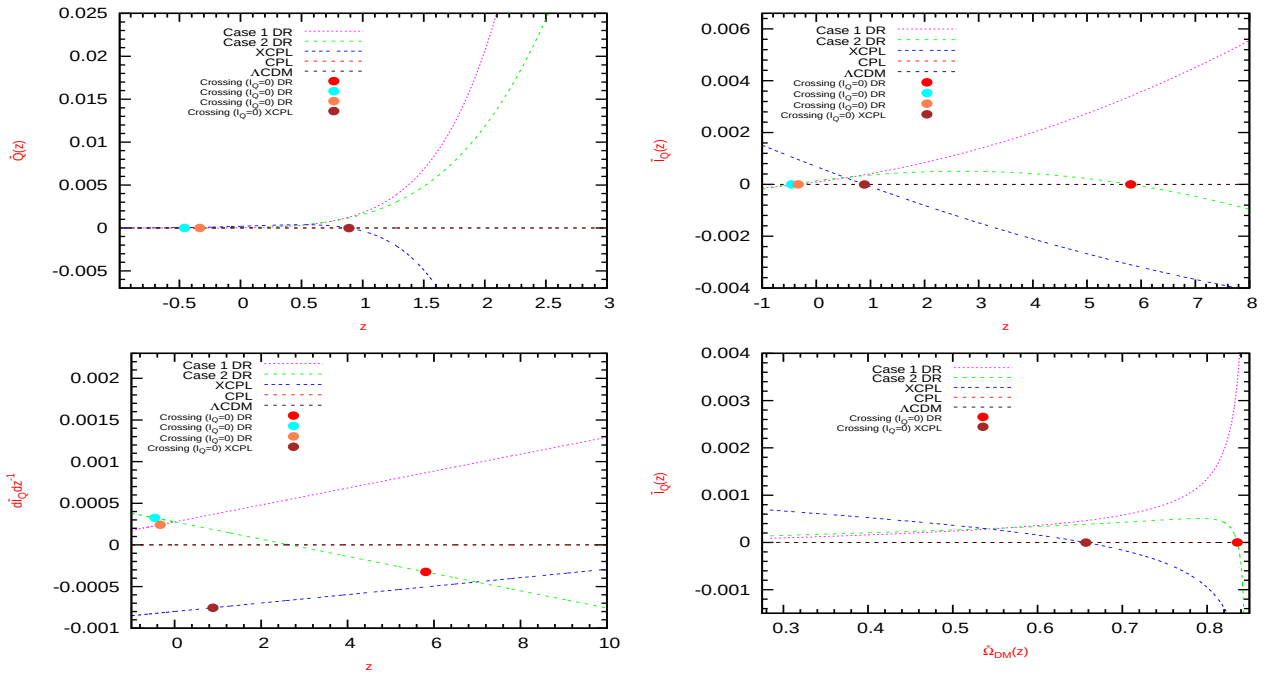

FIG. 2. (color online) The upper panels display the best reconstructed $\bar{Q}(z)$ and $\bar{\mathrm{I}}_{\mathrm{Q}}$ along z. Similarly, the lower panels show the reconstructed evolution of $\mathrm{d}\bar{\mathrm{I}}_{\mathrm{Q}}\mathrm{d}z^{-1}$ in function of z and the effect of $\bar{\mathrm{I}}_{\mathrm{Q}}$ on $\bar{\Omega}_{DM}$, respectively.

could reduce the uncertainty and put tighter constraints on the values of the cosmological parameters. Table IV describes the priors used in this work. For each of the models, the one-dimension probability contours, the best fitting parameters and their errors (at 1σ and 2σ) are shown in Fig. 1.

The values of the functions $f\sigma_8$, γ, $\bar{\mathrm{I}}_{\mathrm{Q}}$, ω, $\bar{\Omega}_{DM}$, G_{eff} and H_{eff} evaluated in $z = 0$ (today) are denoted as $f\sigma_{8,0}$, γ_0, I_0, ω_0, $\bar{\Omega}_{DM,0}$, $G_{eff,0}$ and $H_{eff,0}$, respectively (see Table VI.

In the following Figs. the constraints at 1σ and 2σ on $\bar{\Omega}_{DM}$, $\bar{\Omega}_{DE}$, $\bar{\mathrm{I}}_{\mathrm{Q}}$, ω, $f\sigma_8$, $H_{eff}H^{-1}$, $G_{eff}G^{-1}$ and γ have been omitted to obtain a better visualization of the results.

Let us now see Fig. 2, within the coupled models have considered that I_+ denotes an energy transfer from DE to DM; on the contrary, I_- denotes an energy transfer from DM to DE. In this regard, within the coupled models have found a change from I_+ to I_- and vice versa. A change of sign on the best reconstructed $\bar{\mathrm{I}}_{\mathrm{Q}}$ is linked to the crossing of the non-coupling line, $\bar{\mathrm{I}}_{\mathrm{Q}}(z) = 0$. Table VII shows the $z = z_{crossing}$ points that satisfy the condition $\bar{\mathrm{I}}_{\mathrm{Q}}(z) = 0$, which were already predicted by Eq. (27). Moreover, the left below panel in Fig. 2, confirms the statement given by Eq. (30). We also verify that if the z points satisfy the relation $\mathrm{d}\bar{\mathrm{I}}_{\mathrm{Q}}\mathrm{d}z^{-1}|_z = 0$, then they will be different in comparison with the z_{cross} points. According to Table VI and the upper panels in Fig. 2, note that a non-negligible value of $\bar{\mathrm{I}}_0$ at 1σ error is found in the coupled models, and whose order of magnitude is in agreement with the results obtained in [77–81, 86]. However, due to the two minimums obtained in the DR model (see Table V), two different cases (1 and 2) to reconstruct I_{Q} are worked here. From Table V we focus on the case 2, which is in disagreement with the result obtained in Eq. (35); in this way, the observational data are the fundamental tool to fix the constraints on the cosmological parameters, testing and choosing the possible theoretical models to be worked. On the other hand, from the results presented in Fig. 3, we note that in the left and right above panels the universe evolves from the quintessence regime $\omega > -1$ to the phantom regime $\omega < -1$, and in particular, crosses the phantom divide line $\omega(z_{phantom}) = -1$ [114]. In the DR model, this crossing feature is more favored with two phantom crossing points in $z = z_{phantom\,1} = 0.0155$

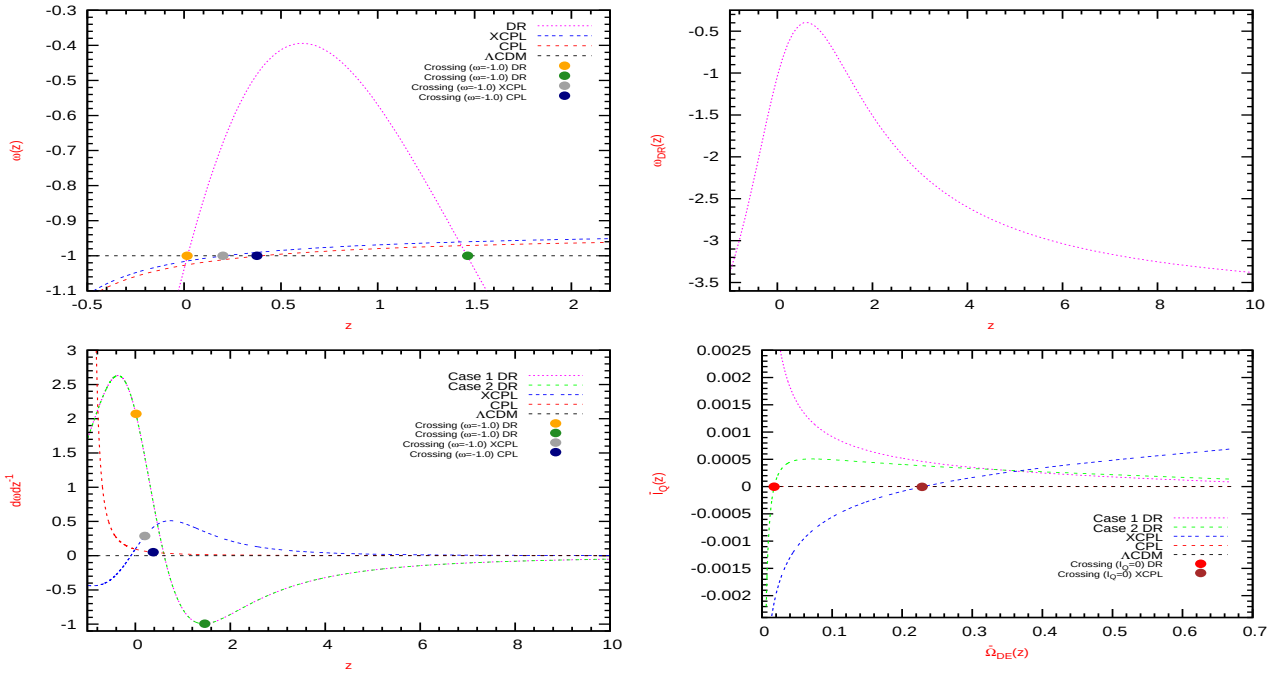

FIG. 3. (color online) The upper panels display the best reconstructed $\omega(z)$ and $\omega_{DR}(z)$ along z. Similarly, the lower panels show the reconstructed evolution of $\mathrm{d}\omega\mathrm{d}z^{-1}$ in function of z and the effect of $\bar{\mathrm{I}}_{\mathrm{Q}}$ on $\bar{\Omega}_{DE}$, respectively.

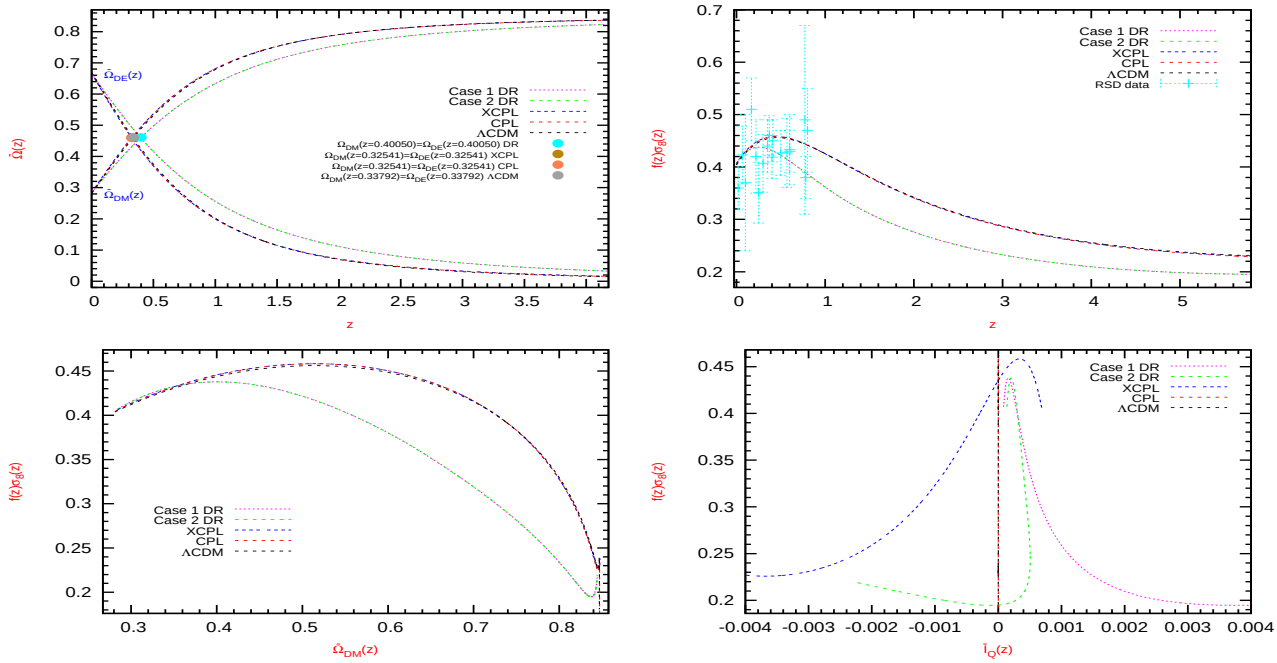

FIG. 4. (color online) The left above panel shows the evolution of $\bar{\Omega}$ along z, whereas the right panel displays the evolution of $f\sigma_8$ as function of z. The left and right below panels depict the evolution of $f\sigma_8$ as function of $\bar{\Omega}_{DM}$ and $\bar{\mathrm{I}}_{\mathrm{Q}}$, respectively.

and $z = z_{phantom\,2} = 1.4643$, respectively, instead, the XCPL model shows only one phantom crossing point in $z = z_{phantom\,3} = 0.2003$. Likewise, the CPL model also depicts one phantom crossing point in $z = z_{phantom\,4} = 0.3755$. From these above panels in Fig. 3, we also see that in the XCPL model the evolution of ω is similar to that in the CPL model; in contrast, the parameter ω defined in the DR model, starts to evolve from the value $\omega = 5\omega_2$ during the matter era and reaches the value $\omega = \omega_0$ in the present time. Likewise,

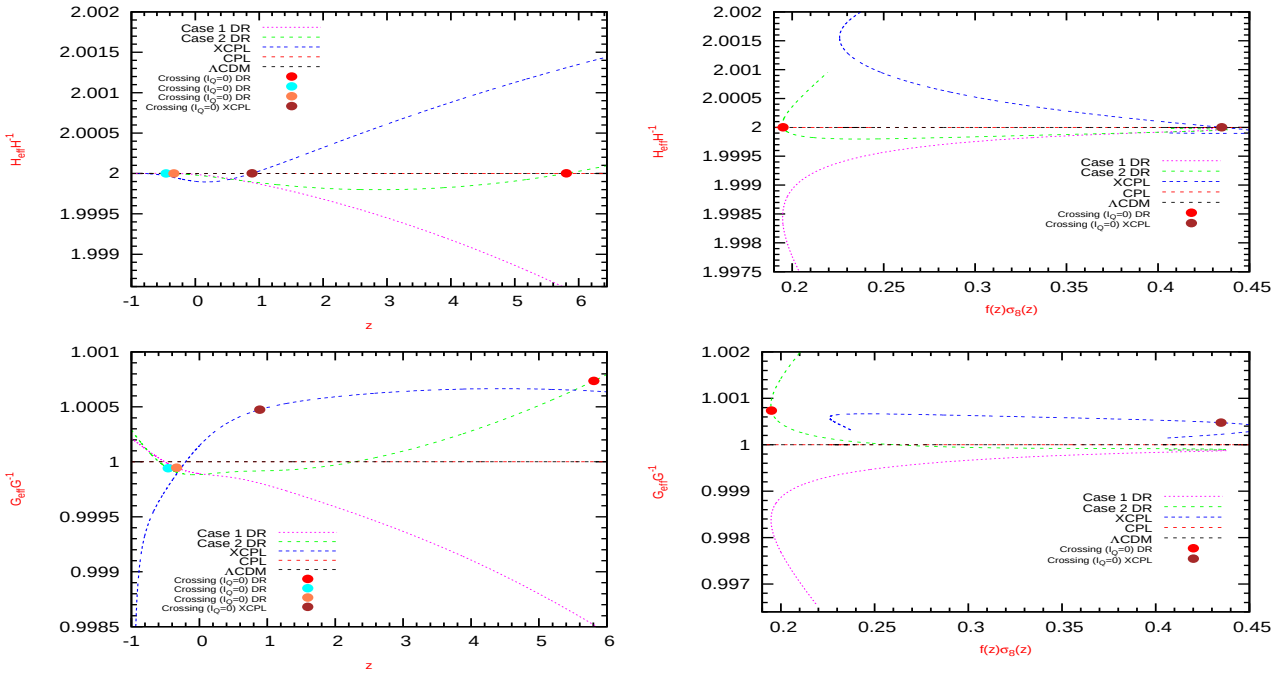

FIG. 5. (color online) The left above panel shows the evolution of $H_{eff}H^{-1}$ along z, whereas the right above panel displays the effect the frictional force on the evolution of $f\sigma_8$. By contrast, the left and right below panels depict the same but for $G_{eff}G^{-1}$.

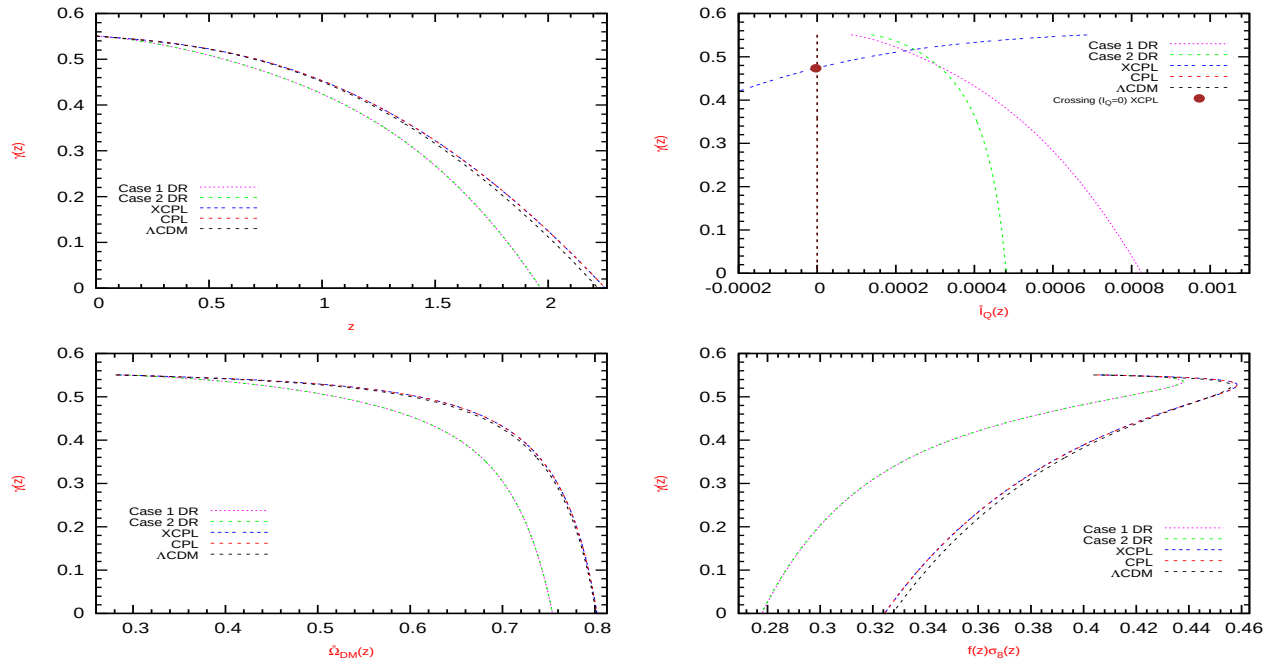

FIG. 6. (color online) The left above panel shows the evolution of γ along z, whereas the right above panel displays the effect of $\bar{\mathrm{I}}_{\mathrm{Q}}$ on the evolution of γ. In addition, the left below panel depicts the effect of $\bar{\Omega}_{DM}$ on γ, and the effect of γ on the cosmic structure formation is shown in the right below panel.

a finite value $\omega(z=-1)=(5/3)\omega_2+(2/3)[\omega_0-\omega_1]$ is obtained in the future. We stress that there is a significant difference for the evolution of ω in the XCPL and DR models, and depend on the epoch at which they are compared. From the right above panel in Fig. 3, we find that in the DR model when $0.6133 \leq z \leq 10$,

the amplitude of ω grows from -3.3799 to -0.3942. By contrast, when $-1.0 < z \leq 0.6133$, the amplitude of ω decreases from -0.3942 to -3.3781, whereas in the XCPL model for $-1 < z \leq 10$, the amplitude of ω decreases more rapidly than that in the DR model. Indeed, these characteristics are a consequence of the reconstructed EoS parameters in the CPL, XCPL and DR models, respectively. In addition, in the DR model for the region $0 \leq z \leq 1.5$, ω deviates significantly from $\omega = -1$, with a pronounced peak at around $z = 0.6133$ and with an average value of $\omega = -0.3942$. This behavior is opposite with the evolution of ω in [117].
From the left below panel in Fig. 3, we also verify that if the z points satisfy the relation $\omega(z_{phantom}) = -1$, then one finds the following condition $\mathrm{d}\omega \mathrm{d}z^{-1}|_{z_{phantom}} \neq 0$.
The right below panels in Figs. 2 and 3, show that $\bar{\mathrm{I}}_{\mathrm{Q}}$ could take positive or negative values during its evolution from -0.0025 to $+0.0025$. Therefore, the values for $\bar{\Omega}_{DM}$ moves from 0.85 to 0.284, and the values for $\bar{\Omega}_{DE}$ moves from 0 to 0.67, respectively. These final values for $\bar{\Omega}_{DM}$ and $\bar{\Omega}_{DE}$ are indicated in Table V.

From the upper panels in Figs. 2 and 3, and from left above panel in Fig. 4, we focus on the DR model at $0.6133 \leq z \leq 10$. Here, ω grows and $\bar{\mathrm{I}}_{\mathrm{Q}}$ could take positive, negative ad null values, and therefore, they will force to the fact that the concentration of Ω_{DE} ($\bar{\Omega}_{DM}$) to grow (decrease) more rapidly than those in the ΛCDM, CPL and XCPL models, respectively. For $-1 < z < 0.6133$, ω decreases and $\bar{\mathrm{I}}_{\mathrm{Q}}$ could take positive, negative and null values. Thus, they will induce to the fact that the values obtained for $\bar{\Omega}_{DE}$ ($\bar{\Omega}_{DM}$) in $z = 0$ are closer to those values measured today, with DE is dominant.
Considering the right above panel in Fig. 2, the right below panels in Figs. 2 and 3, and the left above panel in Fig. 4, we see that for $z \geq 0.3254$ the value of the amplitude of $\bar{\Omega}_{DM}$ ($\bar{\Omega}_{DE}$) in the DR model is slightly modified by the values of $\bar{\mathrm{I}}_{\mathrm{Q}}$ (I_+ and I_-) relative to the other model, it means that, $\bar{\mathrm{I}}_{\mathrm{Q}}$ changes from I_+ to I_-, and vice versa. In this model the amplitude of $\bar{\Omega}_{DM}$ ($\bar{\Omega}_{DE}$) is suppressed (amplified) in comparison with those found in the other models. This result coincides with that found in [74]. Here, we also confirm that the coincidence problem is alleviated in these coupled models, but they may not solve it.
From Table VI and from the below panels in Fig. 5, note that the values of $G_{eff}G^{-1}$ deviate significantly from unity in all z. It is in agreement with the resulted found in [88, 118]. Accordingly, $G_{eff}G^{-1}$ are growing or decreasing functions, and could cross the value $G_{eff}G^{-1} = 1$ at less one time or twice. Furthermore, at $z = 0$, the values of $G_{eff}G^{-1}$ can be roughly larger than 1 (XCPL model) or smaller than 1 (DR model). These observations show the effects of the reconstructions of $\bar{\mathrm{I}}_{\mathrm{Q}}$ and ω on the evolution of $G_{eff}G^{-1}$ in the linear regime. Similarly, considering Table VI, the right above and below panels in Fig. 4 and the upper panels in Fig. 5, find the effect of $\bar{\Omega}_{DM}$ and $\bar{\mathrm{I}}_{\mathrm{Q}}$ on the evolution of $H_{eff}H^{-1}$ function. At around $z = 0$, the values of $H_{eff}H^{-1}$ in the coupled models are roughly different among them. Moreover, for $-1 \leq z \leq 6$ the best fitting of $H_{eff}H^{-1}$ in the XCPL model deviates significantly with respect to that obtained in the DR (cases 1 and 2) model. This is a consequence of the higher quantity of $\bar{\Omega}_{DM}$ concentrated and of a lesser magnitude of $H_{eff}H^{-1}$ in the XCPL model. Therefore, in the region $0 \leq z \leq 6$, the amplitude of $f\sigma_8$ is higher and more pronounced in the XCPL with respect to that in the DR model. At the end of the matter era (at $z \approx 0.4$) the value of $H_{eff}H^{-1}$ in the XCPL model decreases to be approximately smaller than those in the DR and uncoupled models, respectively. In the regime $-0.5 \leq z < 0.4$, the values of $H_{eff}H^{-1}$ in the DR model become closer to 2, and thus higher than those found in the XCPL model, reducing the cosmic structure formation (see right above panel in Fig. 4). Likewise, according to Eqs. (62) and (63) an increase on the magnitudes of $\bar{\mathrm{I}}_{\mathrm{Q}}$ and $\bar{\Omega}_{DE}$ tend to amplify the gravitational strength ($G_{eff}G^{-1}$), but they reduce the magnitude of the frictional force. In fact, an increase in G_{eff} would enhance the growth of structure even at later times.
In addition, the right above and right below panels in Fig. 5, show that $H_{eff}H^{-1}$ ($G_{eff}G^{-1}$) during its evolution could take values from 1.9975 to +2.0020 (from 0.9970 to +1.0020), and therefore the value of $f\sigma_8$ could move from 0.19 to 0.4583. This final value for $f\sigma_8$ is shown in the right upper panel of Fig. 4, and indicated in Table VI.
From Figs. 4 and 5, we consider the evolution of $\bar{\mathrm{I}}_{\mathrm{Q}}$ and $\bar{\Omega}_{DE}$, finding explicitly that in the XCPL model the functions $G_{eff}G^{-1}$ follows a different behavior from that predicted in the DR model. For this reason, the deviations of $G_{eff}G^{-1}$ from standard gravity are significant. It also explains why $f\sigma_8$ is larger in the XCPL model (and uncoupled models) than that in the DR model; especially, when $0 \leq z \leq 6$. More explicitly, for $0 < z < 1$, the values of $G_{eff}G^{-1}$ are close to 1 in the DR model and larger than 1 in the XCPL model, implying the existence of a non-standard gravity. Therefore, in the coupled models the evolution of $\bar{\mathrm{I}}_{\mathrm{Q}}$, $\bar{\Omega}_{DE}$, $\bar{\Omega}_{DM}$ and ω are different such that their effects cannot be ruled out. The modifications to gravity enhance the structure formation at late times in the XCPL models, but suppresses it in the DR model, when $0 \leq z \leq 6$. In general, the deviation of $G_{eff}G^{-1}$ from unity starts at early times ($z \geq 1$) in the coupled models. This indicates that the magnitude of $\bar{\mathrm{I}}_{\mathrm{Q}}$ is very large there. Thus, for $z > 1$, the substantial difference in the values of $G_{eff}G^{-1}$ is more pronounced. In other words, in the XCPL model the matter density is much higher than that in the DR model, and therefore affecting more the magnitude of $f\sigma_8$ in the XCPL model than that in the DR model. This explains why the results are very different in this regime, and the differences from uncoupled models are induced mainly by the effective Hubble friction term, $H_{eff}H^{-1}$ (which acts as a frictional force that slows down the linear structure growth).
The left above panel in Fig. 6, depicts the evolution of γ

along z for the coupled and uncoupled models. Likewise, the right upper and right below panels in Fig. 2, show that $\bar{\mathrm{I}}_{\mathrm{Q}}$ could take positive or negative values during its evolution from $z = 8.0$ to $z = -1$, and the values for $\bar{\Omega}_{DM}$ moves from 0.8 to 0.284. From here, and using the right upper and left below panels in Fig. 6 note that the amplitude for γ is progressively increased to become approximately $\gamma = 0.56$. Additionally, from the right below panel of this Figure and considering the coupled models, note that the values for growth of cosmic structure are very different in the past, and hence the corresponding values for γ are very closed to zero. If the values for $f\sigma_8$ are progressively increased, then the values for γ also increase, and become much more stable, when $\gamma \approx \gamma_0$. In Table VI show the values of γ_0 for each of the models studied.

Let us analyze the right upper and left below panels in Fig. 6. From here, we find that the magnitude of $\bar{\mathrm{I}}_{\mathrm{Q}}$ has imprinted new physical effects on the evolution of the parameter, γ. In the DR model the amplitude of γ is progressively reduced in the region $0 \leq z \leq 2.3$, with respect to those found in the uncoupled models. Therefore, this shows that the magnitude of $\bar{\mathrm{I}}_{\mathrm{Q}}$ is strongly related with the magnitudes of $\bar{\Omega}_{DM}$, $f\sigma_8$ and γ, respectively.

We now compare our results with those obtained by other researchers. In [119], the authors parameterized γ in terms of the Legendre polynomials, and compared it with those obtained from other cosmological models. Here power spectrum data and weak lensing power spectrum data were used. Our results obtained for γ are very closed to that obtained in the $F(R)$ model, at 1σ error. Furthermore, in [120], the authors provided a convenient analytic formula for $f\sigma_8$, which was applied to different DE models. They used RSD data to place observational constraints. The results obtained by them on $f\sigma_8$ are consistent at 1σ error with our results. Likewise, Pouri et al. in [121] used the clustering properties of Luminous Red Galaxies (LRGs) and the growth rate data to constrain γ. The results found by them on γ and $f\sigma_8$ are compatible with our results, at 1σ error. Similarly, Yang and Xu in [122], studied a model composed by the cosmological constant, with a nonzero DM EoS parameter. The result obtained by on $f\sigma_8$ is consistent with our result at 1σ error. Also, the authors in [6], studied the impact of DE clustering on γ. They used two different EoS parameters, and found a fitting evolution curve for $f\sigma_8$, which at 1σ error is acceptable with our result.

IX. CONCLUSIONS

Now we summarize our main results:

• An analysis combined of data was performed to break the degeneracy among the different cosmological parameters of our models, obtaining constraints more stringent on them. In particular, for the XCPL and DR models, the allowed regions for their parameters are significantly reduced by the inclusion of the CMB and RSD data when are compared with studies of models without these data [86]. This implies that higher redshift and dynamical probes may be able to discriminate between these models.

• In the DR model, a novel reconstruction for ω is proposed here, and whose best fitted value is closed to -1. Moreover, it has the property of avoiding divergences in a distant future $z \to -1$. This result is consistent with the value predicted by the ΛCDM model at 1σ error. Likewise, within this coupled scenario, a finite value for ω is obtained from the past to the future; namely, the following asymptotic values are found: $\omega(z) = 5\omega_2$ for $z \gg 1$, $\omega(z) \approx \omega_0$ for $z \ll 1$ and $\omega(z) \approx (5/3)\omega_2 + (2/3)[\omega_0 - \omega_1]$ for $z \to -1$ (see right above panel in Fig. 3). Therefore, a possible physical description performed by the DR model on the dynamical evolution of DE should be used to explore its properties.

• In the coupled models the values of the amplitudes of $\bar{\Omega}_{DE}$ (see left upper panel in Fig. 4) are slightly modified by the reconstructions of $\bar{\mathrm{I}}_{\mathrm{Q}}$ and ω when they are compared with those in the uncoupled models. Nevertheless, they are definitely positive. This requirement implies that ω must be always negative in all the cosmic stages of the universe (see upper panels in Fig. 3).

• If $\bar{\mathrm{I}}_{\mathrm{Q}}$ takes the values I_{+} and I_{-} (see right upper panel in Fig. 2), then the amplitudes of $\bar{\Omega}_{DM}$ ($\bar{\Omega}_{DE}$) (see left upper panel in Fig. 4) for the two cases in the DR model are smaller (larger) in the past than their corresponding $\bar{\Omega}_{DM}$ ($\bar{\Omega}_{DE}$) in the XCPL and uncoupled models. Likewise, we also found in the DR model that the values of the amplitudes of $\bar{\Omega}_{DE}$) are significantly affected by the values of both I_{Q} and ω. Naturally, a smaller proportion of DM leads to a lesser cosmic structure formation. Therefore, the magnitude of $f\sigma_8$ in the DR model is suppressed in comparison with those found in the XCPL and uncoupled models (see right upper panel in Fig. 4).

• For different redshifts, we note that in the coupled models the evolution of $H_{eff}H^{-1}$ and $G_{eff}G^{-1}$ (see Fig. 5) follow different behaviors from those found in the uncoupled models. Therefore, they represent a deviation from the evolution predicted by the uncoupled models. Consequently, the DR model predicts an enhancement (suppression) on the amplitude of $\bar{\Omega}_{DE}$ ($\bar{\Omega}_{DM}$) with respect to that found in the XCPL model (see left upper panel in Fig. 4). These effects are significantly sensible to the reconstructions of $\bar{\mathrm{I}}_{\mathrm{Q}}$ and ω, respectively, and decrease when z tends to zero.

• In the coupled DE models, the decisive role in modifying the cosmic structure formation relative to the uncoupled models is determined mainly by the evolution of $\bar{\mathrm{I}}_{\mathrm{Q}}$, ω and $\bar{\Omega}_{DM}$, respectively. For $z = 0$, the values of $f\sigma_8$ are very closed to each other.

• Currently, an enhancement on the amplitude of $f\sigma_8$ is the situation revealed in XCPL model when it is compared with that in the DR model, and therefore these scenarios should be considered to study new

physical properties of the universe (see right upper panel in Fig. 4).

• The behaviors qualitatively presented here show that the plot for γ has more possibility in discriminating the different coupled DE models, and therefore γ could be used to distinguish them (see left upper panel in Fig. 6).

APENDIXES

Appendix A: Integrals $I_n(z)$ and $\tilde{I}_n(\tilde{x})$

$$I_0(z) = \frac{2}{z_{max}}\left[\ln\left(1+z\right)\right], \tag{A1}$$

$$I_1(z) = \frac{2}{z_{max}}\left[\frac{2z}{z_{max}} - \frac{(2+z_{max})}{z_{max}}\ln\left(1+z\right)\right], \tag{A2}$$

$$I_2(z) = \frac{2}{z_{max}}\left[\frac{4z}{z_{max}}\left(\frac{z}{z_{max}} - \frac{2}{z_{max}} - 2\right) + \left(1+\frac{6.8284}{z_{max}}\right)\left(1+\frac{1.1716}{z_{max}}\right)\ln\left(1+z\right)\right], \tag{A3}$$

$$\tilde{I}_0(\tilde{x}) = \frac{2}{z_{max}}\left[\ln\left(1+0.5\ z_{max}(1+\tilde{x})\right)\right], \tag{A4}$$

$$\tilde{I}_1(\tilde{x}) = \frac{2}{z_{max}}\left[\left(1+\tilde{x}\right) - \frac{(2+z_{max})}{z_{max}}\ln\left(1+0.5\ z_{max}(1+\tilde{x})\right)\right], \tag{A5}$$

$$\tilde{I}_2(\tilde{x}) = \frac{2}{z_{max}}\left[\left(1+\tilde{x}\right)\left(\tilde{x} - \frac{4}{z_{max}} - 3\right) + \left(1+\frac{6.8284}{z_{max}}\right)\left(1+\frac{1.1716}{z_{max}}\right)\ln\left(1+0.5\ z_{max}(1+\tilde{x})\right)\right]. \tag{A6}$$

Appendix B: Quantities A_n and J_n

$$A_0 = \frac{8}{(2+z_{max})^2}\left[\omega_0 - \omega_1 + \omega_2 + 8\omega_2(z_{max}^{-2} + z_{max}^{-1}) - 2\omega_1 z_{max}^{-1}\right], \tag{B1}$$

$$A_1 = \frac{4}{(2+z_{max})^2}\left[\omega_1 - \omega_0 + 5\omega_2 + 16\omega_2(z_{max}^{-2} + z_{max}^{-1}) + 2\omega_1 z_{max}^{-1}\right], \tag{B2}$$

$$A_2 = \frac{4}{(2+z_{max})^2}\left[\omega_0 + 2\omega_1 - 5\omega_2 - 16\omega_2(z_{max}^{-2} + z_{max}^{-1}) + 4\omega_1 z_{max}^{-1}\right], \tag{B3}$$

$$J_0 = \frac{-4}{3(2+z_{max})^2}\left[\lambda_0 - \lambda_1 - \lambda_2 + 2\lambda_2(1+2z_{max}^{-1})^2 - 2\lambda_1 z_{max}^{-1}\right], \tag{B4}$$

$$J_1 = \frac{-2}{3(2+z_{max})^2}\left[-\lambda_0 + \lambda_1 + \lambda_2 + 4\lambda_2(1+2z_{max}^{-1})^2 + 2\lambda_1 z_{max}^{-1}\right], \tag{B5}$$

$$J_2 = \frac{-2\sqrt{2}}{3(2+z_{max})^2}\left[\lambda_0 + 2\lambda_1 - \lambda_2 - 4\lambda_2(1+2z_{max}^{-1})^2 + 4\lambda_1 z_{max}^{-1}\right]. \tag{B6}$$

ACKNOWLEDGMENTS

The author is grateful to Prof. F. Astorga for his academic support and fruitful discussions in the early stages of this research, and also thank Prof. O. Sarbach for useful comments. This work was in beginning supported by the IFM-UMSNH.

[1] Conley A et al., *Astrophys. J. Suppl.* **192** (2011) 1.
[2] Jönsson, J., et al. 2010, *Mon. Not. Roy. Astron. Soc.* **405** (2010) 535.
[3] Betoule M et al., *Astron. and Astrophys.* **568** (2014) A22.
[4] J. C. Jackson, *Mon. Not. Roy. Astron. Soc.* **156** (1972) 1P.
[5] Kaiser N., *Mon. Not. Roy. Astron. Soc.* **227** (1987) 1.
[6] A. Mehrabi, S. Basilakos, F. Pace, *Mon. Not. Roy. Astron. Soc.* **452** (2015) 2930-2939.
[7] Alcock C. and Paczynski B., *Nature.* **281** (1979) 358.
[8] H-J. Seo, E. R. Siegel, D. J. Eisenstein, and M. White, *Astrophys. J.* **686** (2008) 13Y24.
[9] R. A. Battye, T. Charnock and A. Moss *Phys. Rev.* **D 91** (2015) 103508.
[10] L. Samushia, et al., *Mon. Not. Roy. Astron. Soc.* **439** (2014) 3504.
[11] Hudson M. J., Turnbull S. J., *Astrophys. J.* **751** (2013) L30.
[12] Beutler F., Blake C., Colless M., Jones D. H., Staveley-Smith L., et al., *Mon. Not. Roy. Astron. Soc.* **423** (2012) 3430.
[13] Feix M., Nusser A., Branchini E., *Phys. Rev. Lett.* **115** (2015) 011301.
[14] Percival W. J., et al., *Mon. Not. Roy. Astron. Soc.* **353** (2004) 1201.
[15] Song Y.-S., Percival W. J., *J. Cosmol. Astropart. Phys.* **0910** (2009) 004.
[16] Tegmark M. et al., *Phys. Rev.* **D 74** (2006) 123507.
[17] Guzzo L. et al., *Nature.* **451** (2008) 541.
[18] Samushia L., Percival W. J., Raccanelli A., *Mon. Not. Roy. Astron. Soc.* **420** (2012) 2102.
[19] Blake C. et al., *Mon. Not. Roy. Astron. Soc.* **415** (2011) 2876; *Mon. Not. Roy. Astron. Soc.* **418** (2011) 1725.
[20] Tojeiro R., Percival W., Brinkmann J., Brownstein J., Eisenstein D., et al., *Mon. Not. Roy. Astron. Soc.* **424** (2012) 2339.
[21] Reid B. A., Samushia L., White M., Percival W. J., Manera M., et al., *Mon. Not. Roy. Astron. Soc.* **426** (2012) 2719.
[22] de la Torre S., Guzzo L., Peacock J., Branchini E., Iovino A., et al., *Astron. Astrophys.* **557** (2013) A54.
[23] Planck 2015 results, XIII. Cosmological parameters, *Astron. Astrophys.* **594** (2016) A13.
[24] WMAP collaboration, G. Hinshaw et al., *Astrophys. J. Suppl.* **208** (2013) 19.
[25] F. Beutler et al., *Mon. Not. Roy. Astron. Soc.* **416** (2011) 3017.
[26] A. J. Ross et al., *Mon. Not. Roy. Astron. Soc.* **449** (2015) 835.
[27] W. J. Percival et al., *Mon. Not. Roy. Astron. Soc.* **401** (2010) 2148.
[28] E. A. Kazin et al., *Astrophys. J.* **710** (2010) 1444.
[29] N. Padmanabhan et al., *Mon. Not. Roy. Astron. Soc.* **427** (2012) 2132.
[30] C. H. Chuang and Y. Wang, *Mon. Not. Roy. Astron. Soc.* **435** (2013) 255.
[31] C-H. Chuang and Y. Wang, *Mon. Not. Roy. Astron. Soc.* **433** (2013) 3559.
[32] L. Anderson et al., *Mon. Not. Roy. Astron. Soc.* **441** (2014) 24.
[33] E. A. Kazin et al., *Mon. Not. Roy. Astron. Soc.* **441** (2014) 3524.
[34] T. Delubac et al., *Astron. Astrophys.* **574** (2015) A59.
[35] A. Font-Ribera et al., *J. Cosmol. Astropart. Phys.* **05** (2014) 027.
[36] D. J. Eisenstein, W. Hu, *Astrophys. J.* **496** (1998) 605.
[37] D. J. Eisenstein et al., *Astrophys. J.* **633** (2005) 560.
[38] M. D. P. Hemantha, Y. Wang and C-H. Chuang., *Mon. Not. Roy. Astron. Soc.* **445** (2014) 3737.
[39] J. R. Bond, G. Efstathiou and M. Tegmark, *Mon. Not. Roy. Astron. Soc.* **291** (1997) L33.
[40] W. Hu and N. Sugiyama, *Astrophys. J.* **471** (1996) 542.
[41] J. Neveu, V. Ruhlmann-Kleider, P. Astier, M. Besançon, J. Guy, A. Möller, E. Babichev, *arXiv:1605.02627v1.*
[42] G. S. Sharov, *J. Cosmol. Astropart. Phys.* **06** (2016) 023.
[43] C. Zhang et al., *Res. Astron. Astrophys.* **14** (2014) 1221.
[44] J. Simon, L. Verde and R. Jimenez, *Phys. Rev.* **D 71** (2005) 123001.
[45] M. Moresco et al., *J. Cosmol. Astropart. Phys.* **8** (2012) 006.
[46] E. Gastañaga, A. Cabre, L. Hui, *Mon. Not. Roy. Astron. Soc.* **399** (2009) 1663.
[47] A. Oka et al., *Mon. Not. Roy. Astron. Soc.* **439** (2014) 2515.
[48] C. Blake et al., *Mon. Not. Roy. Astron. Soc.* **425** (2012) 405.
[49] D. Stern, R. Jimenez, L. Verde, M. Kamionkowski and S. A. Stanford, *J. Cosmol. Astropart. Phys.* **02** (2010) 008.
[50] M. Moresco, *Mon. Not. Roy. Astron. Soc.* **450** (2015) L16-L20.
[51] N. G. Busca et al., *Astron. Astrophys.* **552** (2013) A96.
[52] P. J. E. Peebles and B. Ratra, *Astrophys. J.* **325** (1988) L17.
[53] P. J. E. Peebles and B. Ratra, *Rev. Mod. Phys.* **75** (2003) 559.
[54] V. Sahni, *Lect. Notes Phys.* **653** (2004) 141.
[55] E. J. Copeland, M. Sami and S. Tsujikawa, *Int. J. Mod. Phys.* **D 15** (2006) 1753.
[56] S. Weinberg, *Rev. Mod. Phys.* **61** (1989) 1.
[57] V. Sahni and A. A. Starobinsky, *Int. J. Mod. Phys.* **D 9** (2000) 373.
[58] U. Seljak, et al., *Phys. Rev.* **D 71** (2005) 103515.
[59] E. Rozo et al., *Astrophys. J.* **708** (2010) 645.
[60] R. R. Caldwell, *Phys. Lett.* **B 545** (2002) 23; S. Nojiri and S. D. Odintsov, *Phys. Lett.* **B 562** (2003) 147; R. Gannouji, D. Polarski, A. Ranquest and A. A. Starobinsky, *J. Cosmol. Astropart. Phys.* **09** (2006) 016; X. Cheng, Y. Gong and E. N. Saridakis, *J. Cosmol. Astropart. Phys.* **04** (2009) 001.
[61] E. Elizalde, S. Nojiri, and S. D. Odintsov *Phys. Rev.* **D 70** (2004) 043539; Z. K. Guo, Y. S. Piao, X. M. Zang and Y. Z. Zhang, *Phys. Lett.* **B 608** (2005) 177.
[62] B. Ratra, and P. J. E. Peebles, *Phys. Rev.* **D 37** (1988) 3406; K. Coble, S. Dodelson, and J. A. Frieman, *Phys. Rev.* **D 55** (1997) 1851; R. R. Caldwell, R. Dave, and P. J. Steinhardt, *Phys. Rev. Lett.* **80** (1998) 1582.
[63] C. Armendariz-Picon, V. Mukhanov, P. J. Steinhardt, *Phys. Rev. Lett.* **85** (2000) 4438, *Phys. Rev.* **D 63** (2001) 103510; T. Chiba, T. Okabe, M. Yamaguchi, *Phys. Rev.* **D 62** (2000) 023511.
[64] A. Y. Kamenshchik, U. Moschella and V. Pasquier, *Phys. Lett.* **B 511** (2001) 265; M. C. Bento, O. Bertolami and A. A. Sen, *Phys. Rev.* **D 66** (2002) 043507; M. K. Mak and T. Harko, *Phys. Rev.* **D 71** (2005) 104022;
[65] M. R. Garousi, M. Sami, S. Tsujikawa, *Phys. Lett.* **B 606** (2005) 1; M. R. Garousi, M. Sami, and S. Tsujikawa, *Phys. Rev.* **D 71** (2005) 083005.
[66] M. S. Turner, *Phys. Rev.* **D 28** (1983) 1243.
[67] K. A. Malik, D. Wands, and C. Ungarelli, *Phys. Rev.* **D 67** (2003) 063516.
[68] R. Cen, *Astrophys. J.* **546** (2001) L77; M. Oguri, K. Takahashi, H. Ohno and K. Kotake, *Astrophys. J.* **597** (2003) 645.
[69] Z. K. Guo, N. Ohta, and S. Tsujikawa, *Phys. Rev.* **D 76** (2007) 023508; L. Amendola, G. C. Campos, R. Rosenfeld, *Phys. Rev.* **D 75** (2007) 083506.
[70] J-H. He and B. Wang, *J. Cosmol. Astropart. Phys.* **06** (2008) 010.
[71] C. G. Böhmer, G. Caldera-Cabral, R. Lazkoz, and R. Maartens, *Phys. Rev.* **D 78** (2008) 023505.
[72] J. Valiviita, E. Majerotto and R. Maartens, *J. Cosmol. Astropart. Phys.* **07** (2008) 020.
[73] S. Campo, R. Herrera and D. Pavon, *J. Cosmol. Astropart. Phys.* **01** (2009) 020.
[74] G. Caldera-Cabral, R. Maartens and B. M. Schaefer, *J. Cosmol. Astropart. Phys.* **07** (2009) 027.
[75] C. G. Böhmer, G. Caldera-Cabral, N. Chan, R. Lazkoz and R. Maartens, *Phys. Rev.* **D 81** (2010) 083003.
[76] L. P. Chimento, *Phys. Rev.*, **D 81** (2010) 043525.
[77] E. Abdalla, L. R. Abramo and J. C. C. de Souza, *Phys. Rev.* **D 82** (2010) 023508.
[78] R. G. Cai and Q. Su, *Phys. Rev.* **D 81** (2010) 103514.
[79] J. H. He, B. Wang, and E. Abdalla, *Phys. Rev.* **D 83** (2011) 063515.
[80] S. Cao, N. Liang and Z. H. Zhu, *Int. J. Mod. Phys.* **D 22** (2013) 1350082.
[81] Y. H. Li and X. Zhang, *Eur. Phys. J. C.* **71** (2011) 1700.
[82] D. Pavón, W. Zimdahl, *Phys. Lett.* **B 628** (2005) 206; D. Pavón, B. Wang, *Gen.Rel.Grav.* **41** (2009) 1-5.
[83] B. Wang, Y. G. Gong and E. Abdalla, *Phys. Lett.* **B 624** (2005) 141.
[84] B. Wang, C. Y. Lin and E. Abdalla, *Phys. Lett.* **B 637** (2006) 357.
[85] S. del Campo, R. Herrera, G. Olivares, and D. Pavón, *Phys. Rev.* **D 74** (2006) 023501.
[86] F. Cueva Solano and U. Nucamendi, *J. Cosmol. Astropart. Phys.* **04** (2012) 011; F. Cueva Solano and U. Nucamendi, *arXiv: 1207.0250* **07** (2012) 02.
[87] W. Zimdahl, *Int. J. Mod. Phys.* **D 14** (2005) 2319.
[88] S. Das, P. S. Corasaniti, and J. Khoury, *Phys. Rev.* **D 73** (2006) 083509.
[89] G. Huey and B. D. Wandelt, *Phys. Rev.* **D 74** (2006) 023519.
[90] B. Wang, J. Zang, C. Y. Lin, E. Abdalla, and S. Micheletti, *Nucl. Phys.* **B 778** (2007) 69.
[91] A. R. Cooray and D. Huterer, *Astrophys. J.* **513** (1999) L95.

[92] M. Chevallier, D. Polarski, *Int. J. Mod. Phys.* **D 10** (2001) 213; E. V. Linder, *Phys. Rev. Lett.* **90** (2003) 091301.
[93] J. Barboza, E. M. and J. Alcaniz, *Phys. Lett.* **B 666** (2008) 415.
[94] E. M. Barboza Jr. et al; *Phys. Rev.* **D 80** (2009) 043521.
[95] Q. J. Zhang and Y. L. Wu, *J. Cosmol. Astropart. Phys.* **08** (2010) 038.
[96] H. Li and X. Zhang, *Phys. Lett.* **B 703** (2011) 119; J. Z. Ma and X. Zhang, *Phys. Lett.* **B 699** (2011) 233.
[97] R. A. Daly and S. Djorgovski, *Astrophys. J.* **597** (2003) 009.
[98] D. Huterer and A. Cooray, *Phys. Rev.* **D 71** (2005) 023506.
[99] A. Shafieloo, U. Alam, V. Sahni and A. A. Starobinsky, *Mon. Not. Roy. Astron. Soc.* **366** (2006) 1081.
[100] A. Hojjati, L. Pogosian and G. B. Zhao, *J. Cosmol. Astropart. Phys.* **04** (2010) 007.
[101] O. Sarbach and M. Tiglio, *Liv. Rev. Rel.* **15** (2012) 9.
[102] E. F. Martinez and L. Verde, *J. Cosmol. Astropart. Phys.* **08** (2008) 023.
[103] Sargent W. L. W. and Turner E. L., *Astrophys. J.* **212** (1977) 3.
[104] Hamilton A. J. S., *"The Evolving Universe". Kluwer Academic* (1998) 185-275.
[105] Peacok J. A. et al., *Nature.* **410** (2001) 169.
[106] Hawkins E. et al., *Mon. Not. Roy. Astron. Soc.* **346** (2003) 78.
[107] A. De Felice, R. Kase and S. Tsujikawa, *Phys. Rev.* **D 83** (2011) 043515.
[108] S. A. Appleby and E. V. Linder, *J. Cosmol. Astropart. Phys.* **08** (2012) 026.
[109] A. De Felice and S. Tsujikawa, *J. Cosmol. Astropart. Phys.* **03** (2012) 025.
[110] Nishimichi T. and Oka. A., *Mon. Not. Roy. Astron. Soc.* **444** (2014) 1400-1418.
[111] Matsubara T. and Suto Y., *Astrophys. J.* **470**, L1 (1996).
[112] Ballinger W. E. Peacok J. A. and Heavens A. F., *Mon. Not. Roy. Astron. Soc.* **282** (1996) 877.
[113] Kazuya Koyama, Roy Maartens, and Yong-Seon Song, *J. Cosmol. Astropart. Phys.* **10** (2009) 017; P. Brax, C. van de Bruck, D. F. Mota, N. J. Nunes, and H. A. Winther, *Phys. Rev.* **D 82** (2010) 083503.
[114] S. Nesseris and L. Perivolaropoulos, *J. Cosmol. Astropart. Phys.* **01** (2007) 018.
[115] E. Majerotto, J. Valiviita and R. Maartens, *Mon. Not. Roy. Astron. Soc.* **402** (2010) 2344.
[116] T. Clemson, K. Koyama, G. B. Zhao, R. Maartens and J. Valiviita *Phys. Rev.* **D 85** (2012) 043007.
[117] S. Nesseris, A. De Felice, and S. Tsujikawa, *Phys. Rev.* **D 82**, (2010) 124054; J. Lu, *Phys. Lett.* **B 680**, (2009) 404; J. Neveu, et al., *Astron. and Astrophys.* **555** (2013) A53.
[118] L. Amendola, *Phys. Rev.* **D 69**, (2004) 103524.
[119] A. Bueno B.,J. Gracia-Bellido, and D. Sapone, *J. Cosmol. Astropart. Phys.* **10** (2011) 01.
[120] S. Tsujikawa, A. De Felice and J. Alcaniz, *J. Cosmol. Astropart. Phys.* **01** (2013) 030.
[121] A. Pouri, S. Basilakos, M. Plionis, *J. Cosmol. Astropart. Phys.* **08** (2014) 042.
[122] W. Yang and L. Xu, *Phys. Rev.* **D 89** (2014) 083517.